TECHNICAL REPORT
NATICK/TR-83/007

ANALYSIS OF ACCELERATIONS IN A DYNAMICALLY LOADED TACTICAL SHELTER

BY
ARTHUR R. JOHNSON III

JULY 1982

UNITED STATES ARMY NATICK
RESEARCH & DEVELOPMENT LABORATORIES
NATICK, MASSACHUSETTS 01760

AERO-MECHANICAL ENGINEERING LABORATORY

UNCLASSIFIED

SECURITY CLASSIFICATION OF THIS PAGE (When Data Entered)

REPORT DOCUMENTATION PAGE

READ INSTRUCTIONS BEFORE COMPLETING FORM

1. REPORT NUMBER: NATICK/TR--83/007
2. GOVT ACCESSION NO.: A124 378
3. RECIPIENT'S CATALOG NUMBER:

4. TITLE (and Subtitle): ANALYSIS OF ACCELERATIONS IN A DYNAMICALLY LOADED TACTICAL SHELTER

5. TYPE OF REPORT & PERIOD COVERED:

6. PERFORMING ORG. REPORT NUMBER: NATICK/TR-83/007

7. AUTHOR(s): Arthur R. Johnson

8. CONTRACT OR GRANT NUMBER(s):

9. PERFORMING ORGANIZATION NAME AND ADDRESS:
US Army Natick Research & Development Laboratories
ATTN: DRDNA-UE
Natick, MA 01760

10. PROGRAM ELEMENT, PROJECT, TASK AREA & WORK UNIT NUMBERS:
62723A, 1L162723A427
01009BG

11. CONTROLLING OFFICE NAME AND ADDRESS:
US Army Natick Research & Development Laboratories
ATTN: DRDNA-UE
Natick, MA 01760

12. REPORT DATE: July 1982

13. NUMBER OF PAGES:

14. MONITORING AGENCY NAME & ADDRESS(if different from Controlling Office):

15. SECURITY CLASS. (of this report): UNCLASSIFIED

15a. DECLASSIFICATION/DOWNGRADING SCHEDULE:

16. DISTRIBUTION STATEMENT (of this Report)

Approved for public release; distribution unlimited.

17. DISTRIBUTION STATEMENT (of the abstract entered in Block 20, if different from Report)

18. SUPPLEMENTARY NOTES

19. KEY WORDS (Continue on reverse side if necessary and identify by block number)

ISO SHELTERS	DYNAMIC ANALYSIS
FINITE ELEMENT ANALYSIS	FREIGHT CONTAINERS
ARMY SHELTERS	CONTAINERS
SHELTERS	TACTICAL SHELTERS

20. ABSTRACT (Continue on reverse side if necessary and identify by block number)

A finite element model used for performing static analyses of a two-for-one tactical shelter was modified so that it could be used for dynamic analyses. Discussions on the construction of the mass matrix and the choice of a proportional damping matrix are given. Low frequency undamped free body vibration mode shapes are determined. Dynamic loads for use in an analysis of an end drop are determined by analyzing a rigid shelter impacting a continuous series of springs at an angle. A time difference between the peak acceleration response at the impact end and at the center of the floor was found both numerically and experimentally.

DD FORM 1 JAN 73 1473 EDITION OF 1 NOV 65 IS OBSOLETE

UNCLASSIFIED

SECURITY CLASSIFICATION OF THIS PAGE (When Data Entered)

20. ABSTRACT (cont'd)

Computed floor stresses for both soft and hard impact surfaces are presented. Data from a Belgian block road test is presented. The Belgian block test is numerically simulated by enforcing a pitching and rolling motion of the ISO fittings (attachment points to the mobilizers). All transient calculations were made by integrating the equations of motion by the Newmark methods using the COSMIC*NASTRAN program.

PREFACE

This work represents part of an effort to develop and use structural design models of tactical shelters. Other efforts involve both the manufacture of and testing of prototype shelters. Past structural design modeling efforts included using a model to predict the static response of a shelter and using a model to suggest changes to the design of prototype shelters so that they would pass transverse racking tests. The author would like to thank Mr. John Roche and Mr. James McLaughlin for their assistance in processing computer runs and plotting data during the early stages of this effort.

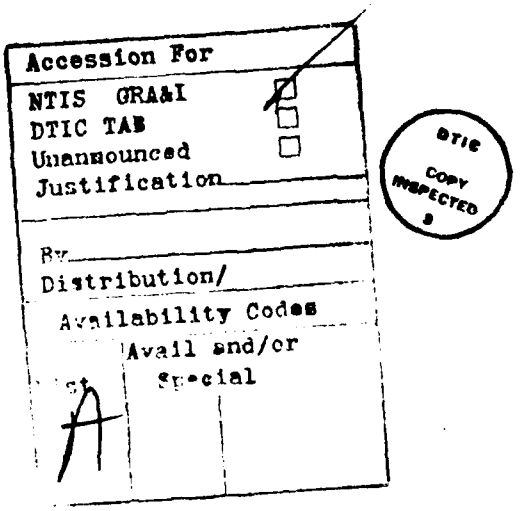

TABLE OF CONTENTS

LIST OF FIGURES

LIST OF FIGURES (cont'd)

LIST OF TABLES

ANALYSIS OF ACCELERATIONS IN A DYNAMICALLY LOADED TACTICAL SHELTER

INTRODUCTION

The Army is currently developing a family of rigid wall tactical shelters. Prototype 2.4 m x 2.4 m x 6.1 m one-side expandable shelters have been designed and fabricated. These shelters are made from extruded aluminum frame members and paper honeycomb/aluminum skin sandwich panels. One of the prototype shelters has undergone environmental and transportation tests to simulate the extreme static and dynamic loads expected when the shelter is shipped.[1] Previous numerical studies have been made to determine the static response of a tactical shelter[2,3] and these results have been compared with the static test data. The comparison of computed and measured accelerations for two of the dynamic tests is the topic of this report. The first test analyzed is the rotational end drop test in which one end of the shelter is placed on a block and the other end is lifted and allowed to drop. The second test analyzed is the Belgian block test in which the shelter is mounted on an ISO mobilizer and towed over a specially prepared road surface. In both of these tests only accelerations were measured.

A finite element model[4] constructed for determining the static response of a one-side expandable tactical shelter is modified in this study for use in dynamic analyses. The construction of the mass matrix, damping matrix and the dynamic loads used in the analyses is discussed.

DESCRIPTION OF THE MASS MATRIX USED

The finite element modeling associated with the elastic response of the two-for-one shelter is described in reference 4. Figures 1 through 5 summarize the mesh pattern and elements used in the finite element model. In this study the mass matrix is defined from design data for the shelter. That is, information on the construction and assembly of the components of the shelter was used to determine the distribution of both structural and nonstructural mass.

[1] "Qualification Test and Demonstration Report for the Natick Laboratories Tactical Rigid Wall One Side Expandable Shelter," Report No. BR 498–26–001, Brunswick Corp., Marion, VA, 1979.

[2] A. R. Johnson and V. P. Ciras, "Finite Element Analysis of a Statically Loaded ISO Tactical Shelter," Technical Report NATICK/TR–79/023, US Army Natick Research and Development Command, Natick, MA, 1979. (AD A075807)

[3] F. D. Barca, "Experimental Measurement of Strain and Acceleration Levels in a Rigid Wall Shelter Subjected to Environmental Loadings," Technical Report NATICK/TR–79/024, US Army Natick Research and Development Command, Natick, MA, 1979. (AD A076606)

[4] A. R. Johnson, "Response of a Two-for-One Tactical Shelter to Racking Loads," Technical Report NATICK/TR–81/016, US Army Natick Research and Development Laboratories, Natick, MA, 1981. (AD A102389)

The total mass in the model of the shelter is the sum of the mass of the plate, beam, and concentrated mass elements used in the model. The mass of the skins in the sandwich panels accounts for only 40 to 50% of the mass of the panel (close-out extrusions not included). Thus, the mass of the structural components of these sandwich panels could not be used alone to represent the inertial properties of the panels. The total mass of each structural panel used in this study is given in Table 1. The total mass was assumed to be uniformly distributed over the panel elements. Nonstructural areal mass densities representative of the total mass of each panel divided by the total area in the finite element model were used to compute panel element mass matrices. The element mass matrices for the beam elements were determined using the cross sectional area and length of the beam elements and the density of aluminum ($2.71 \cdot 10^3$ kg/m^3). Some of the mass from nonstructural items was included as concentrated mass elements. These elements are described in Table 2. The total mass of the finite element model of the shelter used in this study is 2110 kg and the approximate actual mass of the shelter is 2359 kg. The difference is approximately 10% and is probably due to an incomplete account of the nonstructural mass in the shelter.

In the calculations presented in the following sections, lumped mass element matrices were used for all calculations with the exception of the final calculation in the section on the Belgian block test. In that calculation, consistent element mass matrices were used with a load averaging startup technique to help reduce errors near t = o, which are related to having a load vector with large components, and null displacement and velocity vectors at t = 0. The calculation of element mass matrices and the startup method are given in "The NASTRAN Theoretical Manual (Level 17.5)."[5]

LOW FREQUENCY FREE BODY MODE SHAPES

Using the mass and stiffness matrices, the free body vibration modes of the shelter with frequencies under 35.0 Hz were determined. There were 17 modes including the six rigid body modes. The mode frequencies and the major portions of the shelter contributing to the mode shape are given in Table 3. The mode shapes of the 11 elastic vibration modes determined are given in Figures 6 to 16.

The mode shapes shown in Figures 6 to 16 can be related to some details of the finite element model. The expandable side of the shelter involves a number of panels attached to each other through hinges. In particular, the outer wall in the shipping configuration is the fold-out floor. The fold-out floor panel was the only panel on the fold-out side considered as a load carrying panel. The other panels were assumed to be concentrated masses attached to either the top of the fold-out floor, the corner posts, or the edge of the roof. The roof and the fold-out floor panels have mass concentrated along their free edges. One would then expect these panels to have mode shapes that have maximum amplitude at the free edges of the panels (where the stiffness is low and the concentration of mass is high). Figures 6 to

[5] "The NASTRAN Theoreticl Manual (Level 17.5)," NASA SP–221(05), COSMIC, Barrows Hall, University of Georgia, Athens, GA.

10, and 13 demonstrate this behavior. Figure 6 through 8 indicate that the first two modes for the fold-out floor occur before the first mode for the fixed roof. The fact that the fixed roof is nearly clamped along three edges and has a hat beam stiffener under the fourth edge while the fold-out floor is nearly pinned on three edges and has its fourth edge free supports this relationship of the modes. Figures 11, 12, and 14 to 16 show global modes. That is, they represent modes in which many components of the shelter are excited.

The eigenvalue computations necessary for determining the free body mode shapes for this finite element model are costly. Thus, it is worth mentioning a few details about the computer runs made. The technique used to obtain the eigenvectors (mode shapes) is called the inverse power method with shifts. It is a modification of the power method which requires a user specified frequency range (NASTRAN converts this to an eigenvalue range). NASTRAN can implement the inverse power method with shifts to compute all the mode shapes with frequencies in the specified range. It can be requested to determine a given number of mode shapes with frequencies in the specified range. In this study, three computer runs were made to determine low frequency mode shapes. All of the mode shapes were found for the range 0.0 to 35.0 Hz, and all of the elastic undamped free body mode shapes are given in Figures 6 to 16. Six rigid body modes were determined. The cost for creating the global stiffness and mass matrices from scratch, obtaining six mode shapes (eigenvectors), and plotting the mode shapes was about 114 minutes total (77 minutes CPU) in a UNIVAC 1106 computer.

ANALYSIS OF END DROP TEST

The test configuration for an end drop test is shown in Figure 17. The shelter floor is uniformly loaded with a mass of 4536 kg. One end of the shelter is placed on 10.2 cm thick blocks and the other end is lifted 30.0 cm above the ground. The lifted end is then allowed to drop. The analysis of this test uses the mass and stiffness matrices from the modal analysis described above. The model is completed with a load vector and damping matrix which are described here along with the results of the analysis and comparison of these results with experimental results.

Load Vector

To construct a model of the loading, the transient data for an end drop test is used to determine the parameters in a model of the interaction between the ground and the shelter during impact. The first model chosen predicts slightly wider acceleration profiles than were measured. So, a second model of the interaction between ground and shelter was constructed to determine how these acceleration profiles changed when the impact surface is a displacement hardening material (stiffens as it is compressed). These models were used to obtain an impulse force for the finite element analysis of the end drop test.

Mass and stiffness matrices for finite element analysis of structures can be determined a priori to obtaining knowledge of the response of the structure. It is much more difficult to select a damping matrix a priori. Usually, damping matrices are determined for a number of vibration modes. This is done by physically exciting the modes and measuring the decay of the response. Here, proportional damping is used and the constant of proportionality is

determined by varying it until the drop test transient response from the finite element analysis decays similar to the measured response.

The parametric model of the shelter impacting the ground is based on the assumption that the elastic deformations of a shelter during an impact with the ground are small enough for the shelter to be approximated as a rigid body impacting a deformable surface. The model is called a parametric model because restraining forces during the drop and the elastic properties of the ground are not known and are dealt with by adjusting the values (parameters) in the model which represent them. The model is divided into two parts. In the first part the angular velocity of the shelter at the time of impact is determined as a function of the geometry of the test setup. The theoretical "free drop" initial angular velocity is compared to an initial angular velocity obtained by integrating the measured acceleration profiles. In the second part of the analysis the shelter is modeled as a rigid body impacting the ground. The ground is modeled as a continuous series of springs and the properties of the ground are changed until the computed peak acceleration at the impact end of the shelter is approximately the same as the measured acceleration at that end.

The variables used to determine the initial angular velocity are m, g, H and I as indicated in Figure 18. Initially, the shelter is above the elastic surface by a distance H (the drop height) at the end opposite the block. The angular travel of the shelter is assumed small enough for the approximation $\theta \doteq \mathrm{Tan}\theta \doteq \mathrm{Sin}\theta$ to be valid. With $L = 2x_0$ the equation of motion about 0 in Figure 18 (without the elastic surface in contact with the shelter) can be written and solved yielding the following approximation for the angular velocity at impact, $\dot{\theta}_i$.

$$\dot{\theta}_i = \left[\frac{mgH}{I}\right]^{1/2} \tag{1}$$

The experimental data available for a 30.0 cm end drop indicated that equation (1) overestimates the initial angular velocity of the shelter. This fact was determined by comparing results from equation (1) with estimations of the initial angular velocity obtained by numerically integrating the experimental translational accelerations of the shelter at the point of impact. The translational accelerations of the impact end were divided by the length of the shelter so that they would approximate angular accelerations of the shelter. The constant of integration (which is the initial angular velocity at impact) was set so that the final angular velocity of the shelter was zero. Equation (1) predicts an initial angular velocity of 0.48 rad/sec and integration of the measured data indicates a value between 0.25 and 0.34 rad/sec (depending on which experimental curve is integrated). One possible reason for the measured data implying a smaller angular velocity than the free drop calculated value is that the shelter was not allowed to drop freely. The shelter had to pull a free wheeling cable out of the crane. When no experimental data is available, equation (1) can be used to estimate $\dot{\theta}_i$ but the estimate will be high.

The author chose to use the value of 0.25 rad/sec, obtained from the measured data, as the initial angular velocity in the parametric model of the ground and shelter interaction presented next. The results of the parametric study will be different if a different initial angular velocity is used. No estimation of this difference is given here.

The variables shown in Figure 18 can be used to find an approximate solution to the problem of a rotational drop of a rigid shelter onto a surface which is modeled as a continuous series of springs. This is the parametric model of the ground and shelter interaction. The equation of motion for rotation about 0 in Figure 18 is

$$I\ddot{\theta} = mgx_o + T \tag{2}$$

where T = the moment that the deflected springs apply to the shelter (springs in region $\xi \epsilon$ (o, ξ_c) where $\xi = \xi_c$ at the last point of contact between the shelter and the series of springs).

Using Figure 18 we have

$$T = -\int_o^{\xi_c} k(\xi)\ w(\xi)\ (L-\xi)\ d\xi \tag{3}$$

where

$$w(\xi) = (\xi_c - \xi)\ \theta \tag{4}$$

and

$$\xi_c = L - \frac{h}{\theta} = \xi_c(\theta)$$

when $k(\xi) = k$ = a constant, equations (3) and (4) yield

$$T = -k\theta \left[L\xi_c^2 - (L + \xi_c) \frac{\xi_c^2}{2} + \frac{\xi_c^3}{3} \right] \tag{5}$$

Then, equations (2) and (5) yield

$$\ddot{\theta} = \frac{mgx_o}{I} - \frac{k\xi_c^2\theta}{2I} \left(L - \frac{\xi_c}{3}\right) \tag{6}$$

which, using a central difference approximation for $\ddot{\theta}$, yields

$$\theta_{n+1} = 2\theta_n - \theta_{n-1} + \frac{(\Delta t)^2 mgx_o}{I} - \frac{(\Delta t)^2 k\ \xi_{cn}^2\theta_n}{2I} \left(L - \frac{\xi_{cn}}{3}\right) \tag{7}$$

where Δt = the time increment

θ_n = θ at the time $t = n\ (\Delta t)$, $n = 0, 1, 2, \ldots$

and ξ_{cn} = ξ_c at time $t = n\ (\Delta t)$

Several values of k, the ground constant, were tried until an acceleration vs time profile (for the end of the shelter which hits the ground first) resulted which was similar to the experimental results already obtained. Then, data was obtained for multiple and fractional values of this k to observe how the acceleration profiles change as the properties of the ground change. The resulting data for acceleration vs time is presented in Figure 19. Also, the torque applied to the shelter by the continuous series of springs (a measure of the dynamical force) was computed and is shown in Figure 20. Thus, Figure 20 can be used to determine dynamical

loads for changes in the specification of the end drop test for which the impact surface responds in a manner similar to the compression of an elastic surface during impact.

In addition to the analysis of the ground and shelter interaction made in the parametric study above the following analysis of a shelter impacting a spring whose stiffness depends on its displacement was also made. This analysis was made to determine how the shape of the acceleration profile would change if the ground became stiffer as it was deformed. Using Figure 21 the equation of motion for rotation about O is

$$I\ddot{\theta} = mgx_o - k(x)L \tag{8}$$

Using a central difference approximation for $\ddot{\theta}$ and letting

$$a_1 = (\Delta t)^2 \frac{L^2}{I} \tag{9}$$

$$a_2 = -(\Delta t)^2 \frac{mgx_o}{I} \tag{10}$$

and

$$f_\theta = k\,(L\theta)\,\theta. \tag{11}$$

The finite difference scheme for determining successive values of θ is

$$\theta_{n+1} = 2\theta_n - \theta_{n-1} - a_1\, f_{\theta n} - a_2 \tag{12}$$

Using equation (12) and an initial condition on $\dot{\theta}_i$ of 0.47 rad/sec the curves shown in Figure 22 were generated. These curves show how the profile of the dynamic force changes if the ground becomes harder as it deforms. The results indicate that, if the ground stiffens as it is deformed, the pulse starts more slowly, ends sooner, and is much larger in maximum value.

The torque curve associated with ground constant of k in Figure 20 was used with a half period of 0.05 sec to determine concentrated dynamic loads of the form

$$F = A \sin(2\pi ft),\ F = 0 \text{ for } t > \frac{1}{2f} \tag{13}$$

which were applied in the vertical direction to nodes 400, 411, 422, 433, and 444 (the impact end of the shelter). The loads give the same peak value of the total dynamical torque applied to the shelter and have the same overall pulse time. The loads, however, are broader in shape than the associated acceleration profiles.

Damping Matrix

The determination of a useful model of structural damping is required before computations of the transient response of the shelter for impulse loads (ground and shelter interaction) are made. Here, the impulse load determined by the parametric model described above is modeled as a sine-shaped pulse. The measured accelerations indicated that the pulse length should be about 0.05 sec. The peak value of the pulse and the time at which the peak occurred varied

with location on the shelter. After the initial impulse each acceleration curve looked similar to the acceleration profile of a near critically damped one degree of freedom system. Thus, a structural damping matrix was needed which would simulate to near critically damped structure. The determination of a damping matrix via experimental techniques was beyond the scope of this effort. The following numerical study was made to determine a range of damping matrices which would numerically simulate the near critically damped characteristics observed in the measured data.

Next, with [K] = the stiffness matrix, a proportional damping matrix, [B], of the form

$$[B] = \rho\ [K] \tag{14}$$

where ρ = a constant was computed. Using the force given by equation (13), a number of analyses of the shelter response were made for different values of ρ in equation (14) and Δt (the time increment for the Newmark integration scheme in NASTRAN). The results are shown in Figure 23. It was difficult to construct the plot of the experimental data shown in Figure 23 because the best plot of the experimental data obtainable was on a much more compact time scale. However, the computed acceleration profiles at both the impacting end (point of load application) and at the center of the floor were definitely broader than the measured acceleration profiles.

The plots in Figure 23 indicate that damping constants ρ = 0.0063 and ρ = 0.0100 both gave near critically damped acceleration profiles. Also, Figure 23 shows that when the time increment Δt = 0.0050 sec was cut in half to Δt = 0.0025 sec the computed accelerations did not change significantly. The peak value of the acceleration near the center of the floor was too high for the damping constant ρ = 0.0 and ρ = 0.0010. Both damping values of ρ = 0.0063 and 0.0100 were used for the computations discussed in the remainder of this report and any value in this range is considered useful for analysis of the end drop in gravel. The value of ρ used for the calculations is shown on the figures containing the results.

Comparison of Computed and Measured Accelerations

Two dynamic loads determined above were used to generate acceleration profiles at points on the shelter where data were measured. The two loads are shown in Figure 24. The tabulated load was obtained by taking the profile for the impulse load for a ground constant $k = k_o x$ in Figure 22 and scaling it so that its peak value was the same as the peak value for the harmonic load. Note that these two forces yield different momentum changes of the shelter. One can then criticize using these two load profiles for analysis of the end drop simply because they imply different momentum changes of the shelter. However, since we do not accurately know the momentum of the shelter at impact, we cannot choose one profile over the other. The output of the finite element analysis using the harmonic load versus the tabulated load were as close as their profiles show in Figure 24. Thus, there was no loss in accuracy for this problem, due to using a tabulated load (that is, NASTRAN functioned well for both types of loads). Only the results for the harmonic load were compared to the measured data. In the calculation for comparison to the measured data, the harmonic force shown in Figure 24 was applied to each node at the impact end of the shelter: nodes 400, 411, 422, 433, and 444 as shown in Figure 2. The value of ρ was 0.0063 and the time increment was 0.0050 sec in the calculation.

The locations of the points on the shelter where the accelerations were measured are shown in Figure 25. Each point is given a channel number associated with the measured data. The global node numbers associated with these points are also shown. Figure 26 shows the measured accelerations and the accelerations resulting from integrating the finite element equations of motion using the harmonic dynamic load.

The measured acceleration profiles shown in Figure 26 were obtained by smoothing the curves presented in reference 1 and approximating the smoothed curves on graph paper suitable for plotting the computed accelerations. The curves presented in reference 1 were already electronically smoothed by a 180 Hz filter. The magnitude of the impulses between 50 and 180 Hz were very small (10% of the low frequency impulses at the impact end) and the smoothed curves presented here are a good representation of the low frequency response of the shelter during the end drop. In general, the computed accelerations agree well with the measured accelerations. The peak values decrease in magnitude as the point location varies from the impact end to the pivot end. The pulse time is approximately correct for all points except the center of the roof. Inspection of the measured profile at channel 8 in Figure 26 indicates that the center of the roof is apparently experiencing an underdamped vibration with a frequency of about 33 Hz. This is not unreasonable considering the free body undamped vibration modes of the shelter indicate the roof has excitation modes (with the center of the roof not a vibration node) at 11.5, 31.0, 33.2, and 34.4 Hz respectively (see Figures 8, 14, 15, and 16). The observed 10 Hz damped vibration response of the expandable floor is not close in frequency to any of the undamped vibration modes of the shelter in which the center of the expandable floor is active. Comparison of the times at which the profiles peak for channels 1, 4, and 6 (see Figure 26) indicate that both the measured and computed profiles predict a time difference of $\Delta t = 0.012$ sec for peaks at channels 1 and 4 vs the peak at channel 6. That is, the response at the center of the floor lags the response at the impact end by a time shift of approximately 0.012 sec.

Dynamic Stresses in the Center of the Floor for Soft and Hard Impact Surfaces

To demonstrate how dynamic loads for both soft and hard surfaces can be obtained from Figure 20 and used in design studies, the following comparison of floor skin stresses was made for impacts on soft and hard surfaces. Elements 420 and 424 (impact end and center of floor) were chosen for stress output. The dynamic load used to represent an impact on a soft surface was the harmonic load used above. To model the impact on a hard surface the analysis of a rigid shelter impacting a single spring (see Figure 21) was used. An initial angular velocity of 0.247 rad/sec. The maximum force in the spring was then known. The nodal dynamical forces applied to nodes 400, 411, 422, 433, and 444 are as follows.

Soft impact surface: maximum surface deflection = 3.25 cm

$$f = 6.23 \times 10^4 \ N \ \mathrm{Sin}[2\pi(10.0)t] \qquad 0 \leq t < 0.05 \text{ sec} \qquad (15)$$

$$= 0.0 \qquad 0.05 \leq t < \infty \text{ sec}$$

Hard impact surface: maximum surface deflection = 0.64 cm

$$f = 1.79 \times 10^5 \; N \; \sin[2\pi(40.3)t] \qquad 0 \leq t < 0.0124 \text{ sec} \qquad (16)$$

$$= 0.0 \qquad 0.0124 \leq t < \infty \text{ sec}$$

The Hencky-Von Mises stress vs time in the top skin at the center of elements Nos. 420 and 424 are shown in Figures 27 and 28 for both soft and hard impact surfaces. Comparing equations 15 and 16 we see that the hard surface dynamic load was nearly three times as large and occurs in about 1/4 the time as the soft surface load. The stress profiles indicate that the maximum Hencky-Von Mises stress in the top skin of the sandwich floor panels in elements 420 and 424 increase by a factor of 2 when the impact surface changed from soft to hard. That is, in this case, the ratio of the amplitudes of the dynamic loads was about 3/1 and this resulted in a ratio of maximum stresses of about 2/1. We note, however, that the two loads used do not cause the shelter to experience identical momentum changes. The loads do represent estimates of the dynamic loads a shelter would experience when impacting a soft or hard surface, and the calculations indicate that the stresses for and loads for different impact surfaces are not proportional to the accelerations. Thus, each different impact load requires integration of the equations of motion.

ANALYSIS OF THE BELGIAN BLOCK TEST

Description of Test and Measured Accelerations

The Belgian block test is a road transporation test in which the shelter and payload have a gross mass of 4,536 kg. The loaded shelter is mounted on mobilizers, see Figure 29, and is towed over an irregular bumpy surface with crests placed to subject the shelter to both pitching and rolling motions.

A two-for-one shelter was subjected to road transporation tests by the Materiel Testing Directorate at Aberdeen Proving Ground during December 1978. A portion of the testing included the measuring of accelerations at a number of locations on the shelter and on the mobilizers shown in Figure 30. The test data was recorded on two magnetic tapes (each had 14 tracks). A voice channel and a time channel were simultaneously recorded on each tape. Thus, data from all the accelerometers could be compared in the time domain. The data on these two tapes was copied onto one tape which was sent to NLABS. Using this tape (and a written description of what the tape contained) brush recorder pen plots of the measured accelerations were made by personnel of the Experimental Analysis and Design Division in the Aero-Mechanical Engineering Laboratory at NLABS.

Measured accelerations for a common 3.0-sec period of time are presented in Figure 31. The accelerations were measured in vertical, transverse, and longitudinal planes. The profiles consist of both low and high frequency pulses. Channels 1, 3, 4, 5, 6, 7, 10, 13, 16, 17, 18, and 24 have acceleration profiles which are characterized by a superposition of low frequency pulses of one magnitude with high frequency pulses of a smaller magnitude. At channels 2, 8, 11, 12, 14, 19, 20, and 23, the responses are characterized by a superposition of low and

high frequency pulses of similar magnitude, and the responses of channels 9, 15, and 21 by a superposition of low frequency pulses of one magnitude with high frequency pulses of much larger magnitude.

The measured accelerations in each plane were not recorded with respect to a given direction in that plane. For example, a positive acceleration in the transverse direction for one accelerometer may imply an acceleration from the fixed side of the shelter to the expandable side of the shelter while for another, it may imply an acceleration in the opposite direction. Knowledge of the direction of the accelerations is required if information on dynamic deformations of the shelter (for example, dynamic racking) is to be estimated from the measured accelerations. Thus, this dynamic analysis could not be based on knowledge of the dynamic deformations of the shelter.

Model of Belgian Block Test and Computed Accelerations

The purpose of the Belgian block test is to subject the shelter to both pitching and rolling motions. The dynamic model of the shelter traveling over the Belgian block surface used here is an enforcement of pitching and rolling motions of the shelter attained by controlling the motion of the ISO corner fittings. The computer model simulates the shelter's motion as a superposition of pitching and rolling motions enforced by the ISO fittings (attachment points to the mobilizers).

The transverse accelerations at channels 2 and 14 (see Figures 30 and 31) measured very small accelerations compared to channels 4 and 17. This means that the top of the shelter moves transversely while the bottom of the shelter does not. Then an axis for rolling accelerations was chosen to be along the longitudinal centerline of the floor. Similarly, since the longitudinal accelerations measured at channels 3 and 15 were smaller than those at channels 6 and 18 the axis for pitching accelerations was chosen to be along the transverse center line of the floor. These axes are shown in Figure 32.

To obtain estimates of the angular pitching and rolling accelerations about the pitching and rolling axes some of the measured data was used. The assumed location of the pitching and rolling axes described above along with an assumption of small rotations implies that the transverse acceleration measured on channel 5 is a rolling acceleration and that the longitudinal acceleration measured on channel 6 is a pitching acceleration. The measured acceleration data for a common 1.0 sec interval of time at channels 4 and 6 was read from the pen plots at time intervals of 0.02 sec. A table of acceleration vs time data was then available for each gauge. This data was used to obtain a numerical approximation of the pitching and rolling motions. These motions were assumed to be of a harmonic form. Although this is not true for a long period of time, it is shown below that it is possible to approximate the accelerations at channels 5 and 6 (rolling and pitching respectively) by SINE functions for a time period of 0.33 sec. This time period equals 1−1/2 cycles of the SINE function for channel 6 and nearly one full cycle for the SINE function at channel 5.

The tabulated data for each channel was stored in the computer in paired form (y_i, t_i) where y_i = the acceleration at time t_i. The assumed functional form of the data was

$$y = A\ \mathrm{Sin}(\omega t + \phi) \tag{17}$$

where A, W, and ϕ are to be numerically selected for a best fit as measured by least squares. The least squares functional was

$$F = \sum_{i=1}^{N} [A\ \mathrm{Sin}(\omega t_i + \phi) - y_i]^2 \tag{18}$$

A minimum of F was obtained using the Newton-Raphson method. The gradient of F is

$$g = \begin{bmatrix} \frac{\partial F}{\partial A} \\ \\ \frac{\partial F}{\partial \omega} \\ \\ \frac{\partial F}{\partial \phi} \end{bmatrix} \tag{19}$$

where

$$\frac{\partial F}{\partial A} = \Sigma 2[A\ \mathrm{Sin}(\omega t_i + \phi) - y_i]\ \mathrm{Sin}(\omega t_i + \phi) \tag{20}$$

$$\frac{\partial F}{\partial \omega} = \Sigma 2[A\ \mathrm{Sin}(\omega t_i + \phi) - y_i]\, A t_i\ \mathrm{Cos}(\omega t_i + \phi) \tag{21}$$

$$\frac{\partial F}{\partial \phi} = \Sigma 2[A\ \mathrm{Sin}(\omega t_i + \phi) - y_i]\, A\ \mathrm{Cos}(\omega t_i + \phi) \tag{22}$$

The Hessian of F is

$$[H] = \begin{bmatrix} \frac{\partial^2 F}{\partial A^2} & \frac{\partial^2 F}{\partial \omega \partial A} & \frac{\partial^2 F}{\partial \phi \partial \omega} \\ \\ & \frac{\partial^2 F}{\partial \omega^2} & \frac{\partial^2 F}{\partial \phi \partial \omega} \\ \\ (\mathrm{Sym}) & & \frac{\partial^2 F}{\partial \phi^2} \end{bmatrix} \tag{23}$$

where

$$\frac{\partial^2 F}{\partial A^2} = \Sigma 2\ \mathrm{Sin}^2(\omega t_i + \phi) \tag{24}$$

$$\frac{\partial^2 F}{\partial\omega\partial A} = \Sigma 2[2At_i \text{ Sin}(\omega t_i + \phi) \text{ Cos}(\omega t_i + \phi) - y_i t_i \text{Cos}(\omega t_i + \phi)] \quad (25)$$

$$\frac{\partial^2 F}{\theta\phi\partial A} = \Sigma 2[2A \text{ Sin}(\omega t_i + \phi)\text{Cos}(\omega t_i + \phi) - y_i \text{ Cos}(\omega t_i + \phi)] \quad (26)$$

$$\frac{\partial^2 F}{\partial\omega^2} = \Sigma 2[A^2 t_i^2 (\text{Cos}^2(\omega t_i + \phi) - \text{Sin}^2(\omega t_i + \phi)) + At_i^2 y_i \text{ Sin}(\omega t_i + \phi)] \quad (27)$$

$$\frac{\partial^2 F}{\partial\phi\partial\omega} = \Sigma 2[A^2 t_i (\text{Cos}^2(\omega t_i + \phi) - \text{Sin}^2(\omega t_i + \phi) + At_i y_i \text{ Sin}(\omega t_i + \phi)] \quad (28)$$

and

$$\frac{\partial^2 F}{\partial\phi^2} = \Sigma 2[A^2 (\text{Cos}^2(\omega t_i + \phi) - \text{Sin}^2(\omega t_i + \phi)) + y_i \text{ A Sin}(\omega t_i + \phi)] \quad (29)$$

A FORTRAN program was written to use equations (19) through (29) in the Newton-Raphson scheme given by the following equation

$$\begin{bmatrix} A \\ \omega \\ \phi \end{bmatrix}_{j+1} = \begin{bmatrix} A \\ \omega \\ \phi \end{bmatrix}_j - [H]_j^{-1} [g]_j \quad (30)$$

Where the subscript j identifies the j'th approximation.

The results of the analysis are shown in Figures 33 and 34. The data taken at channel 5 fit well to a SINE function for the entire 1.0 sec interval. When the data for channel 6 was fit over the entire 1.0 sec interval shown in Figure 34, the SINE function determined by the least squares fit was out of phase with the measured data for at least 0.25 sec (or 1/4 of the interval). The largest accelerations shown in Figure 34 occurred in the central region and this region was selected for determining a SINE function. The resulting SINE function was in phase with the measured data and was selected for modeling the pitching accelerations.

As shown in Figures 33 and 34, the nonlinear least squares analysis implies that the following functions can be used to model rolling and pitching accelerations (measured in g's).

$$A = 0.9255 \text{ SIN } (16.52t + 1.033) \text{ (rolling)} \quad (31)$$

and

$$A = 0.3784 \text{ SIN } (26.41t + 1.933) \text{ (pitching)} \tag{32}$$

Multiplying the amplitudes of the rolling and pitching accelerations in equations 31 and 32 by the acceleration due to gravity at sea level (9 78049 m/sec^2) and dividing by the normal distance to the rolling and pitching axes (see Figures 30 and 32), we obtain the following rolling and pitching angular accelerations.

$$\theta_1 = 7.4256 \text{ SIN } (16.42t + 1.033) \quad \frac{\text{rad}}{\text{sec}^2} \tag{33}$$

$$\theta_2 = 1.2142 \text{ SIN } (26.41t + 1.933) \quad \frac{\text{rad}}{\text{sec}^2} \tag{34}$$

where θ_1 = the rolling angular acceleration

and θ_2 = the pitching angular acceleration.

The external loads applied to the shelter are applied at the ISO fittings by the mobilizers. The accelerations at these load input points can be approximated with the aid of equations (33) and (34). In this study the dynamic response of the shelter is determined by enforcing the accelerations at the load input points in such a way that the equations of motion can be integrated to obtain the dynamic elastic response of all the other points in the model. A technique for performing such an enforcement of accelerations with the NASTRAN program has been suggested by the developers of the program.[6] In summary, the technique requires that a large mass (or rotational inertia) be assigned to the variables which must have their acceleration enforced. Then, a force equal to the large mass times the enforced acceleration is applied for each of these variables. The required enforced accelerations will be approximately observed along with the associated response of the rest of the model. One requirement on the magnitude of the large mass is that it must be large enough for the relative admittance of the variables associated with it to be much larger than the relative admittance of the rest of the variables in the model. A second requirement is that its admittance not be so large that it numerically uncouples the enforced variables from the response variables in the equations of motion.

One of the objectives of this effort is to develop a dynamical structural model of the Belgian block test so that it can be used in design studies. To compute the response of the shelter, the accelerations at all the load input points (in one global reference system) are needed. This information is not currently available from test data. Also, these accelerations will be dependent on the construction of the shelter itself. That is, if the design of the shelter is changed, then the accelerations at the load input points will also change. In this study a

[6]MSC/CDC 600 NASTRAN Applications Manual, section 2.7, MacNeal-Schwendler Corp., LA, 1978.

preliminary dynamic structural model of the Belgian block test is made by assuming that the eight ISO fitting load input points move as if they are part of a rigid body exposed to the acceleration field imposed by equations (33) and (34). The technique for enforcing accelerations described above is explored by varying the magnitude of the large masses placed at the load input points and observing the computed response.

Assuming rigid body motion of the eight ISO fittings and the acceleration of the rigid body imposed by equations (33) and (34) the acceleration at each ISO fitting can be computed as follows:

$$\vec{a}_N = \vec{\omega} \times (\vec{\omega} \times \vec{\rho}_N) + \vec{\alpha} \times \vec{\rho}_N \tag{35}$$

where $\vec{\alpha} = \ddot{\theta}_1 x_1 + \ddot{\theta}_2 x_2$ = the angular acceleration of the shelter.

$\vec{\omega}$ = the harmonic angular velocity (integrate $\vec{\alpha}$ with the condition that there is no constant or linear terms in the angular velocity).

$\vec{\rho}_N$ = the position vector of the Nth ISO fitting with respect to the axes of rotation (see Figure 32).

A FORTRAN program was written to use equation (35) and to calculate the three components of force at the ISO fitting locations. It was found that the term $\vec{\alpha} \times \rho_N$ in equation (35) dominated the results to two significant figures, as a result the first term in equation (35) was dropped. This proved very useful since it allowed the forces to be implemented in NASTRAN with the TLOAD2 harmonic load option. With (x_1^N, x_2^N, x_3^N) as the coordinates of the Nth ISO fitting and m, the large mass placed at the ISO fitting, the enforced load, $\vec{F}_N$, for the Nth ISO fitting was calculated as follows:

$$\vec{F}_N = m \det \begin{vmatrix} x_1 & x_2 & x_3 \\ \ddot{\theta}_1 & \ddot{\theta}_2 & o \\ x_1^N & x_2^N & x_3^N \end{vmatrix} \tag{36}$$

or $\vec{F}_N = m (\vec{\alpha} \times \vec{\rho}_N)$ (37)

Each of the nonzero components of force given by equation (37) were computed for each of the eight ISO fittings on the shelter and were used as the driving forces for a dynamic analysis of the entire shelter. Several values of the large mass placed at each ISO fitting location were used to obtain the data shown in Table 4. The data shows the effects that the magnitude of the large mass has on the accuracy of the computed accelerations. These results indicate, for this particular structural model, that using a mass of approximately 10^6 times the mass of the shelter results in enforced and elastic accelerations valid to four or more significant digits. Also, the use of a mass of approximately 10^{12} times the mass of the shelter does not destroy the integration of the equations of motion.*

*These calculations were made using lumped mass matrices.

To demonstrate the computationally enforced pitching and rolling motion Figures 35 and 36 were constructed.** In these figures the computed transverse, longitudinal, and vertical accelerations of the ISO fittings are shown. Superposition of the pitching and rolling can be seen in the vertical acceleration profiles. Most of the elastic accelerations indicated a near rigid-body type of motion of the shelter. However, the fold-out floor (which is hinged to the fixed floor, pinned to the corner posts and free at the top) was deforming and not following the rigid-body-like motion of the rest of the shelter. Figure 37 shows the transverse accelerations of a point on the center edge of the roof and of a point on the top center edge of the fold-out floor.

The computed accelerations are not compared to the measured accelerations (except that the fit required by Figures 33 and 34 was satisfied) because the phase of the measured data is not known. This model can be used to determine dynamic loads on connections and dynamic stresses in extrusions and panels subject to the enforced pitching and rolling motions of the ISO fittings described above. However, before this would be economical, specific objectives for the design calculations must be set (for example, a failure of or an intended redesign of a specific component).

CONCLUDING REMARKS

A finite element model has been made and used to compute the dynamic response of a two-for-one tactical shelter. Low frequency, undamped, free-body vibration mode shapes of the shelter were determined. A model of a rigid shelter impacting a continuous series of springs at an angle was used with measured acceleration profiles to generate dynamic loads for a transient analysis of an end drop test. A simulation of the Belgian block road test was made by assuming that the ISO fittings move as if the shelter was rigid, and was rolling and pitching about axes along the center lines of the fixed floor. The characteristics of the pitching and rolling motion were based on curve fits to measured acceleration data at one top ISO fitting. The elastic accelerations of the remainder of the shelter were determined subject to the pitching and rolling motions of the ISO fittings.

For the end drop test both measured and computed data indicate that the maximum stress at the center of the floor occurs at a later time than the maximum stress at the impact end. This implies that when designing shelters to resist loadings imposed by drop tests, more accurate estimates of internal load distributions will be obtained if a dynamic analysis is made instead of the more commonly used method of applying a static "g" load. This is due to the fact that the deformations resulting from the application of the static "g" loading can be significantly different from the time dependent deformations.

The techniques used in this study can be used to analyze the response of the shelters to other drop and road tests. Either determination of the dynamical loads imposed on the shelter or knowledge of the acceleration field at support points is required for each test to be analyzed.

**The consistent mass matrices and a load averaging start-up method was used to generate the data presented in Figures 35 and 36. See the section on the mass matrix for more information.

Two errors in the COSMIC level 17.5 NASTRAN program were found in this study. In one case both multipoint constraints and single point constraints were specified for a common set of variables. It is recognized that this is a user error; however, NASTRAN did not give the user an error message or a warning. In the second case, phase angles were specified for time dependent loads in the Belgian block test (to represent the phase relationship between rolling and pitching). After several computer runs, it was determined that NASTRAN was ignoring the phase angles specified for the loads. The phase shift between the roll forces and pitch forces was enforced by shifting the time coordinates for each load type.

REFERENCES

1. "Qualification Test and Demonstration Report for the Natick Laboratories Tactical Rigid Wall One Side Expandable Shelter," Report No. BR 498–26–001, Brunswick Corp., Marion, VA, 1979.

2. A.R. Johnson and V.P. Ciras, "Finite Element Analysis of a Statically Loaded ISO Tactical Shelter," Technical Report NATICK/TR–79/023, US Army Natick Research and Development Command, Natick, MA, 1979 (AD–A075808).

3. F.D. Barca, "Experimental Measurement of Strain and Acceleration Levels in a Rigid Wall Shelter Subjected to Environmental Loadings," Technical Report NATICK/TR–79/024, US Army Natick Research and Development Command, Natick, MA, 1979 (AD AO76606).

4. Arthur R. Johnson, "Response of a Two-for-One Tactical Shelter to Racking Loads," Technical Report NATICK/TR–81/016, US Army Natick Research and Development Laboratories, Natick, MA, 1981 (AD A102389).

5. "The NASTRAN Theoretical Manual (Level 17.5)," NASA SP–221(05), COSMIC, Barrows Hall, University of Georgia, Athens, GA.

6. MSC/CDC 600 NASTRAN Applications Manual, Section 2.7, MacNeal-Schwendler Corp., LA, 1978.

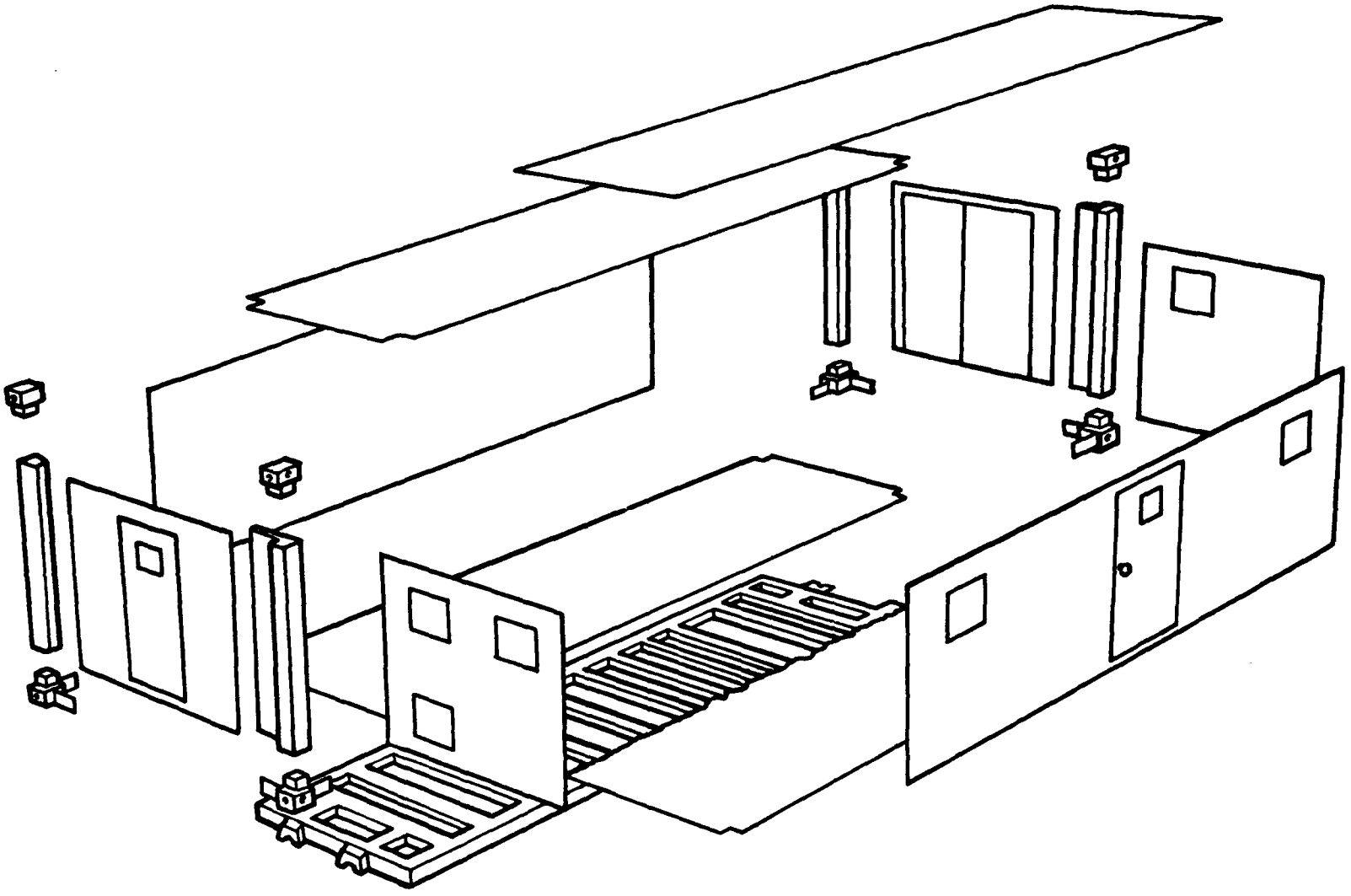

Figure 1. Shelter components used in finite element model.

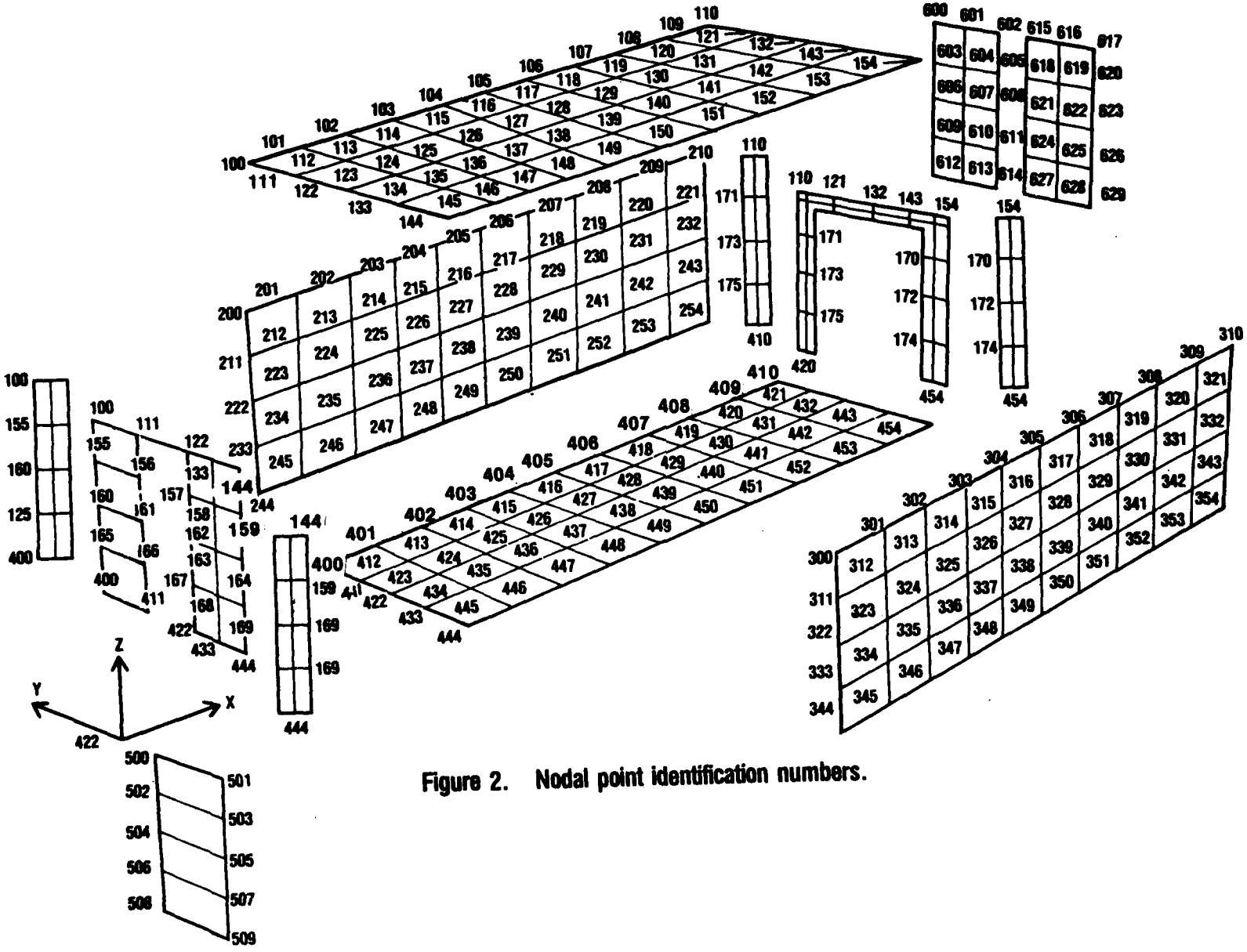

Figure 2. Nodal point identification numbers.

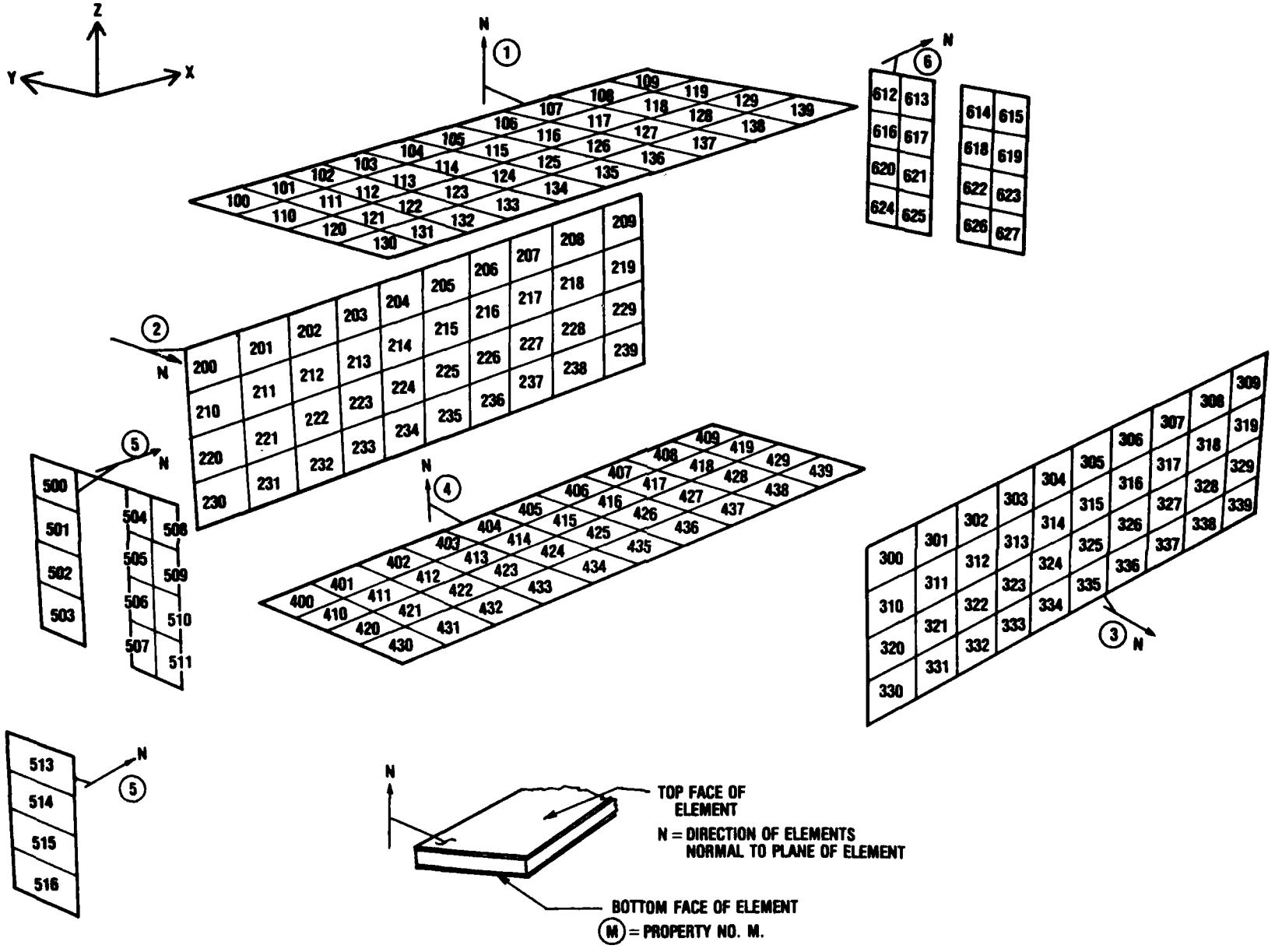

Figure 3. Quadrilateral plate element numbers.

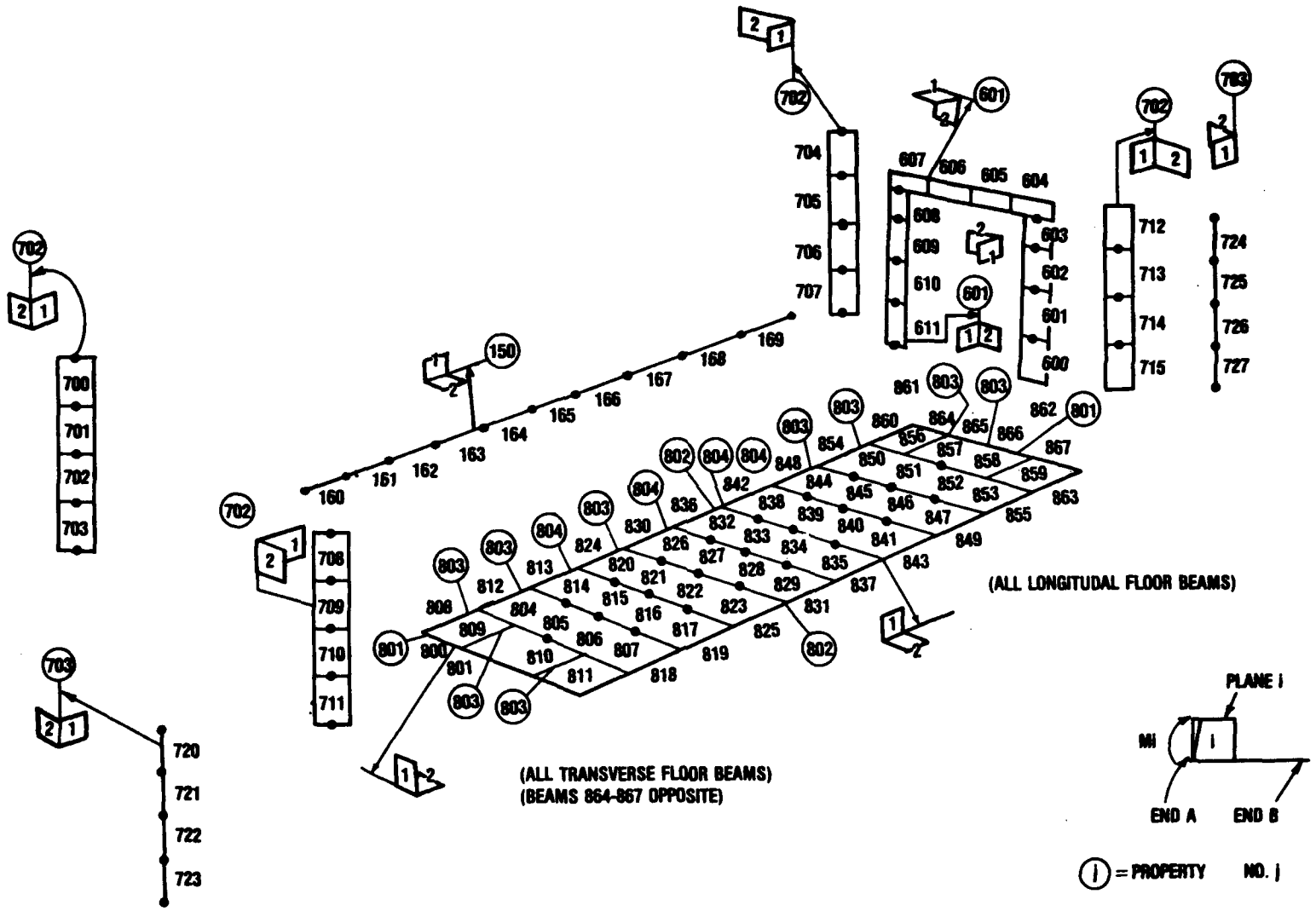

Figure 4. Beam element numbers for frame.

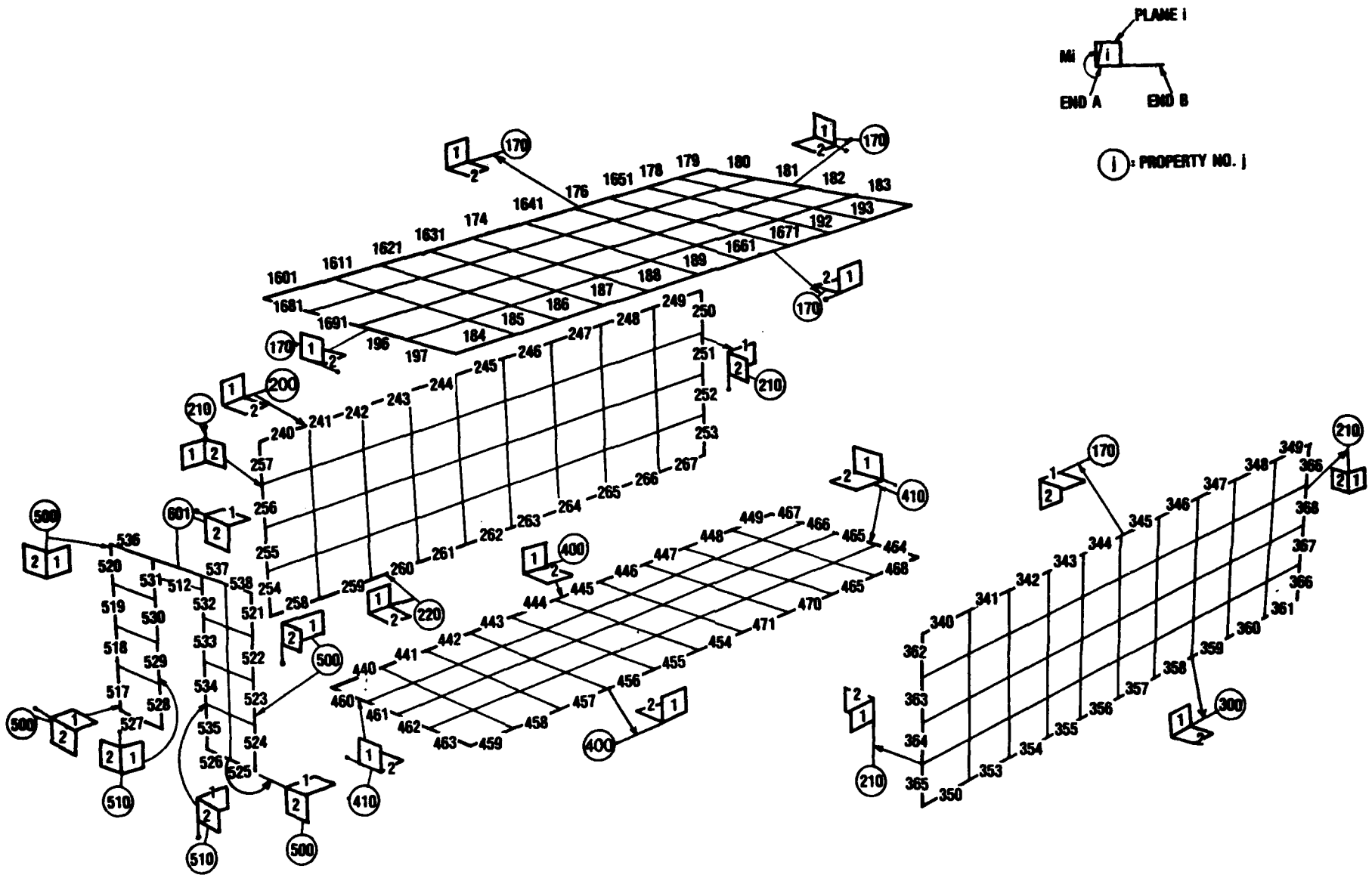

Figure 5. Beam element numbers for panel close-out extrusions.

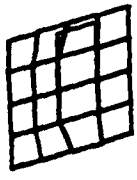

PERSONNEL DOOR WALL

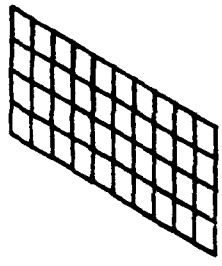

FIXED SIDE WALL

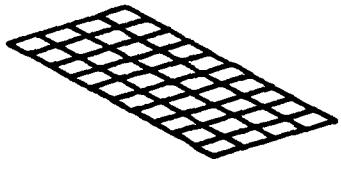

FIXED FLOOR

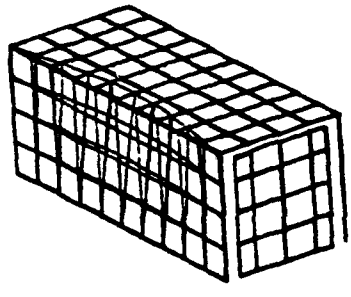

ROOF, FOLD-OUT FLOOR
CARGO DOOR WALL

FIGURE 6. FREE BODY VIBRATION MODE SHAPE, FREQUENCY 4.49 Hz

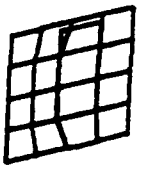

PERSONNEL DOOR WALL

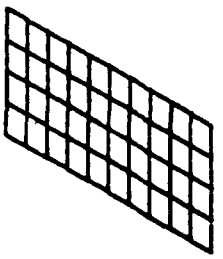

FIXED SIDE WALL

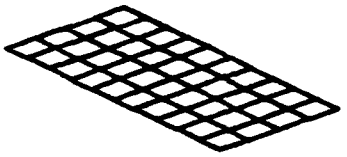

FIXED FLOOR

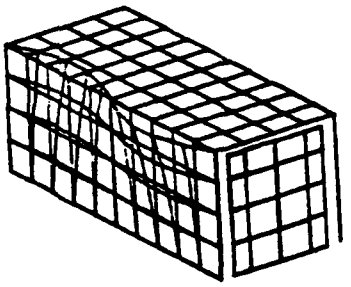

ROOF, FOLD-OUT FLOOR
CARGO DOOR WALL

FIGURE 7. FREE BODY VIBRATION MODE SHAPE, FREQUENCY 10.9 Hz

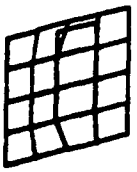

PERSONNEL DOOR WALL

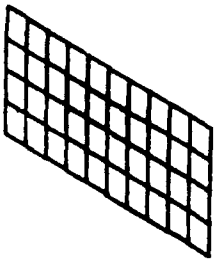

FIXED SIDE WALL

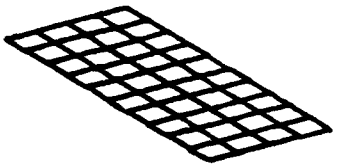

FIXED FLOOR

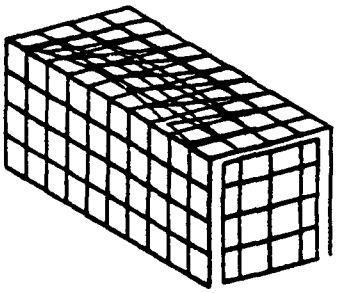

ROOF, FOLD-OUT FLOOR
CARGO DOOR WALL

FIGURE 8. FREE BODY VIBRATION MODE SHAPE, FREQUENCY 11.5 Hz

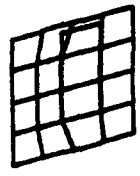

PERSONNEL DOOR WALL

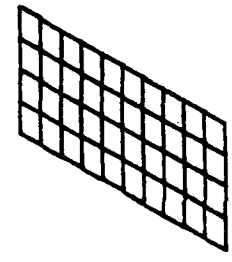

FIXED SIDE WALL

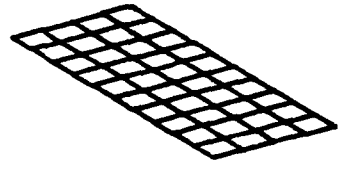

FIXED FLOOR

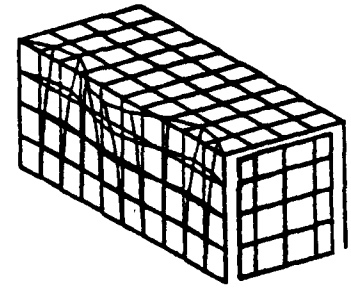

ROOF, FOLD-OUT FLOOR
CARGO DOOR WALL

FIGURE 9. FREE BODY VIBRATION MODE SHAPE, FREQUENCY 20.0 Hz

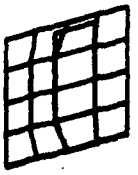

PERSONNEL DOOR WALL

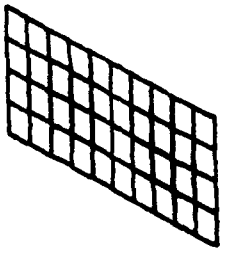

FIXED SIDE WALL

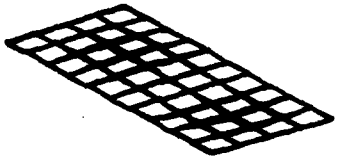

FIXED FLOOR

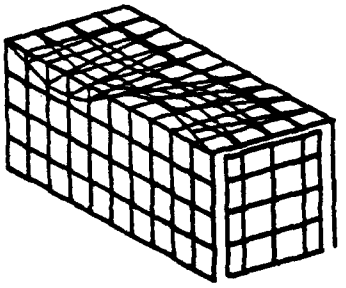

ROOF, FOLD-OUT FLOOR
CARGO DOOR WALL

FIGURE 10. FREE BODY VIBRATION MODE SHAPE, FREQUENCY 25.47 Hz

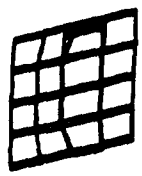

PERSONNEL DOOR WALL

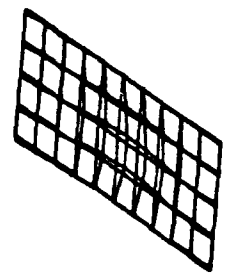

FIXED SIDE WALL

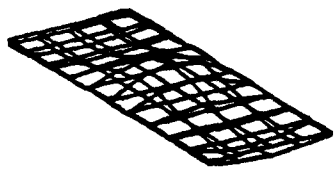

FIXED FLOOR

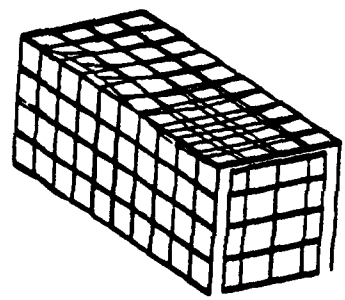

ROOF, FOLD-OUT FLOOR
CARGO DOOR WALL

FIGURE 11. FREE BODY VIBRATION MODE SHAPE, FREQUENCY 26.4 Hz

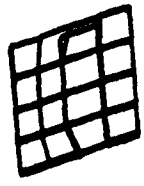

PERSONNEL DOOR WALL

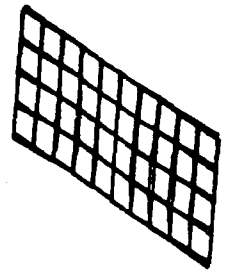

FIXED SIDE WALL

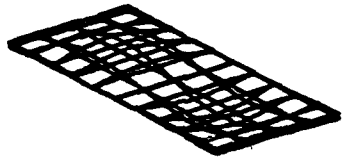

FIXED FLOOR

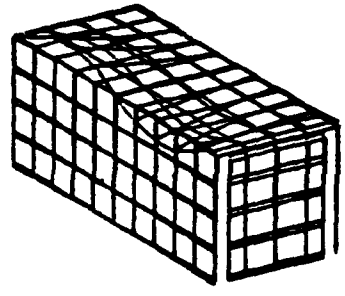

ROOF, FOLD-OUT FLOOR
CARGO DOOR WALL

FIGURE 12. FREE BODY VIBRATION MODE SHAPE
FREQUENCY 27.5 Hz

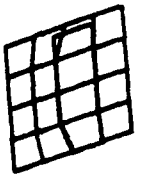

PERSONNEL DOOR WALL

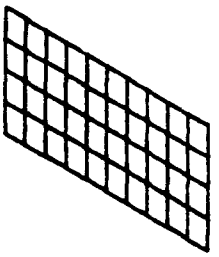

FIXED SIDE WALL

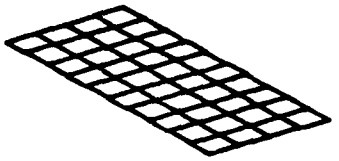

FIXED FLOOR

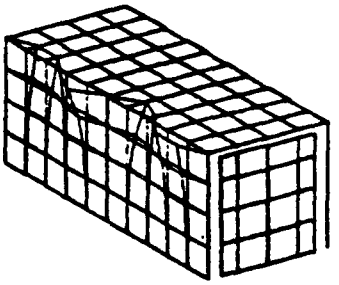

ROOF, FOLD-OUT FLOOR
CARGO DOOR WALL

FIGURE 13. FREE BODY VIBRATION MODE SHAPE, FREQUENCY 29.1 Hz

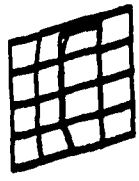

PERSONNEL DOOR WALL

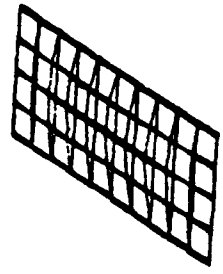

FIXED SIDE WALL

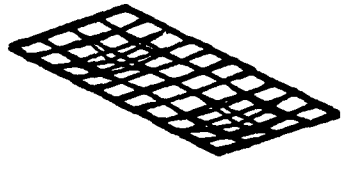

FIXED FLOOR

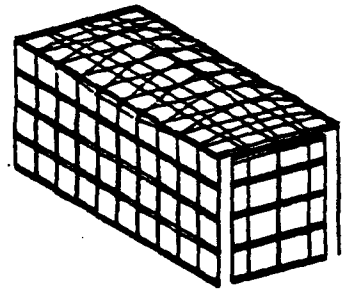

ROOF, FOLD-OUT FLOOR
CARGO DOOR WALL

FIGURE 14. FREE BODY VIBRATION MODE SHAPE, FREQUENCY 31.0 Hz

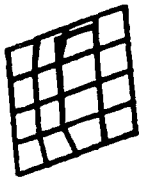

PERSONNEL DOOR WALL

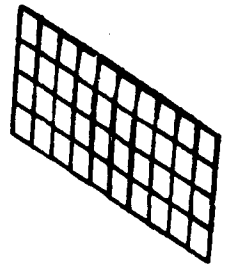

FIXED SIDE WALL

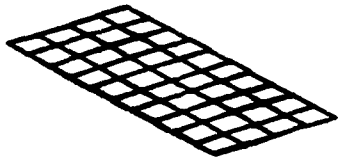

FIXED FLOOR

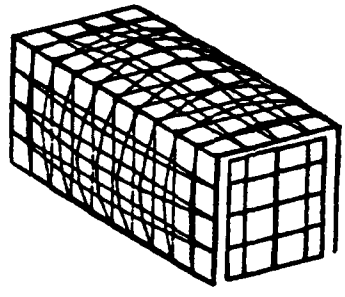

ROOF, FOLD-OUT FLOOR
CARGO DOOR WALL

FIGURE 15. FREE BODY VIBRATION MODE SHAPE, FREQUENCY 33.7 Hz

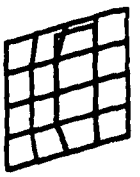

PERSONNEL DOOR WALL

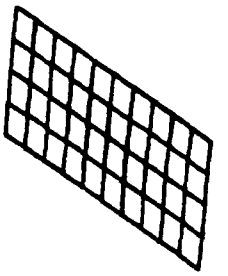

FIXED SIDE WALL

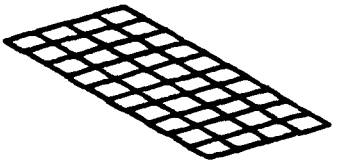

FIXED FLOOR

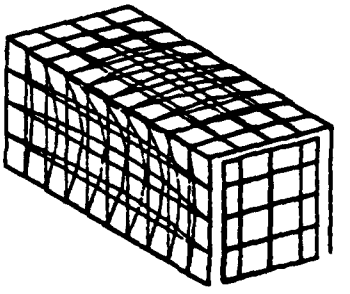

ROOF, FOLD-OUT FLOOR
CARGO DOOR WALL

FIGURE 16. FREE BODY VIBRATION MODE SHAPE, FREQUENCY 34.4 Hz

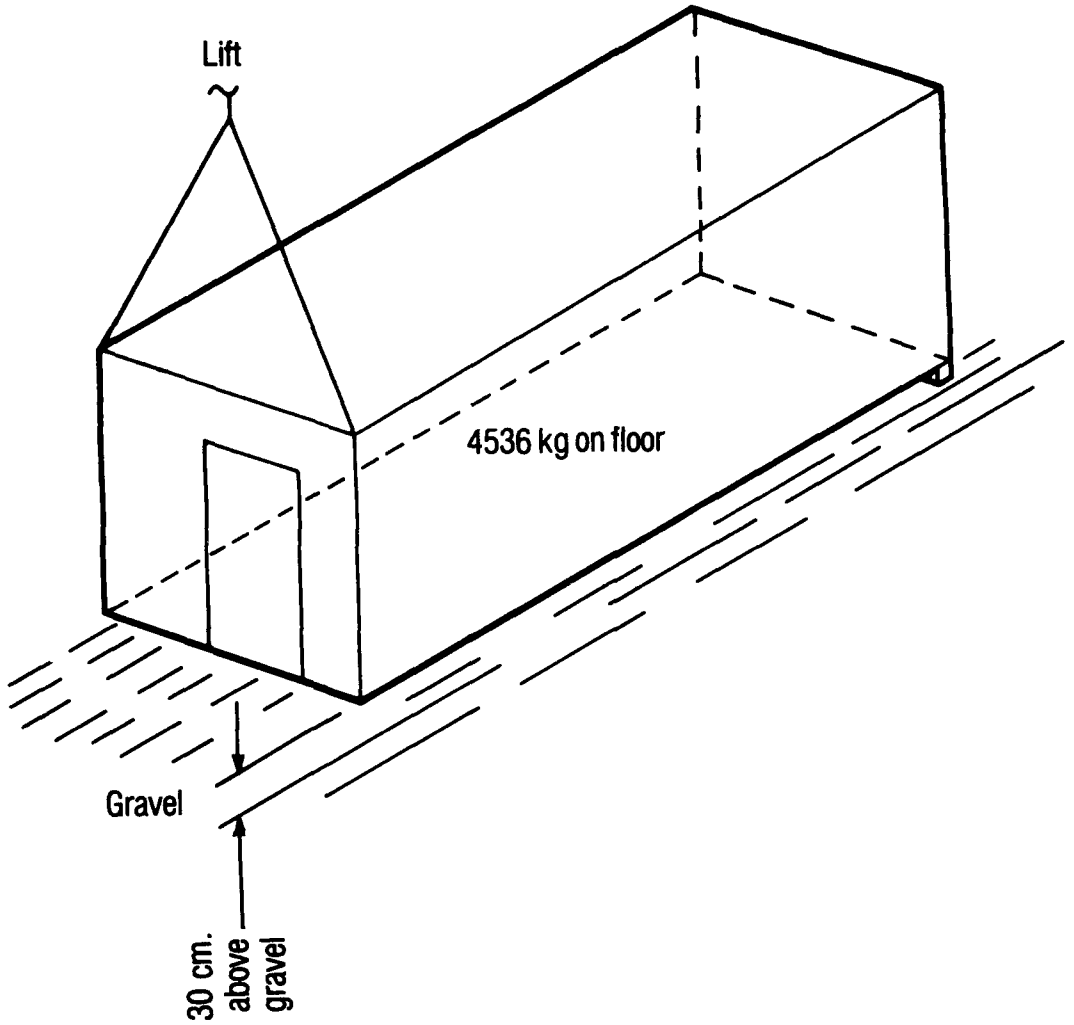

Figure 17. Shelter end drop test.

h = Block height (0.1016 m)

L = Length of shelter (6.096m)

x_0 = Location of center gravity (2.972 m)

ξ, θ = Coordinates

ξ_c = ξ at last point of contact between ground and shelter

$w(\xi)$ = Deflection of ground at ξ

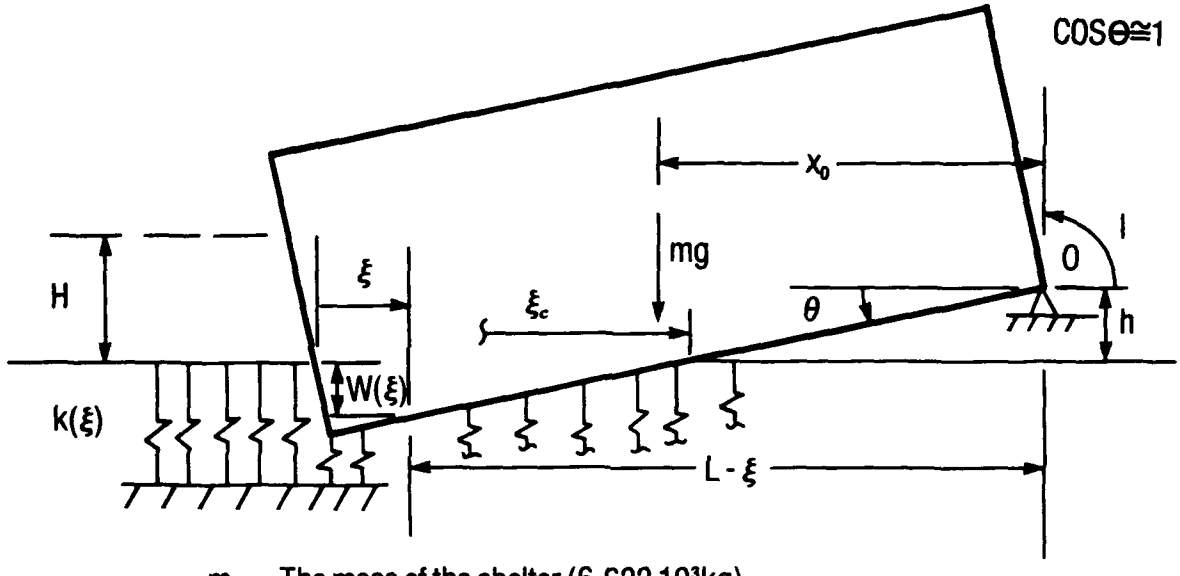

m = The mass of the shelter ($6.622\ 10^3$kg)

I = Moment of inertia about 0 ($8.574\ 10^4$kg m^2)

$k(\xi)$ = The ground spring constant per unit length

g = The acceleration due to gravity

H = Drop height (0.3048 m)

Figure 18. Variables for one dimensional analysis of end drop test, ground modeled as a continuous series of springs.

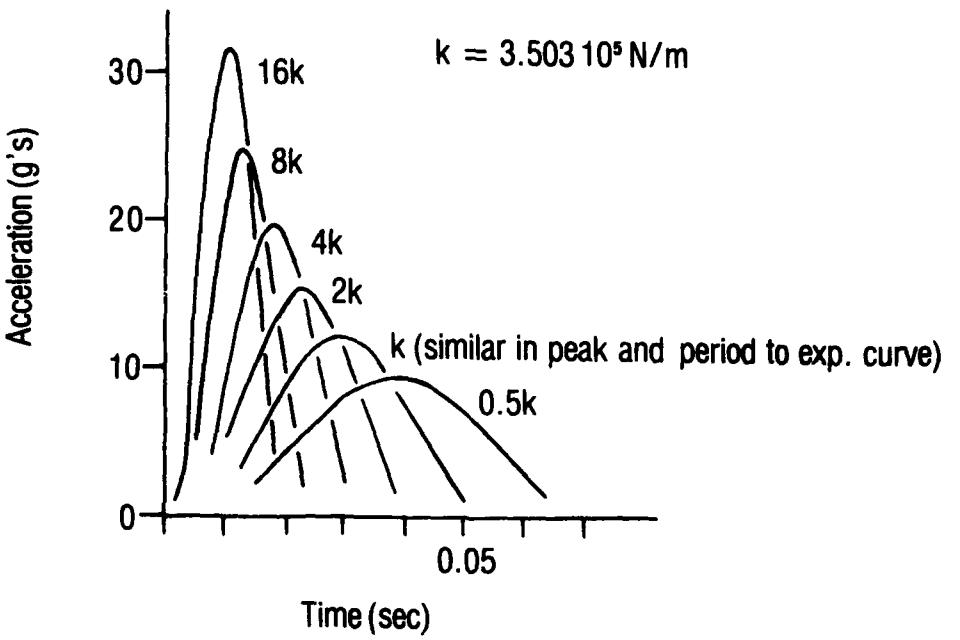

Figure 19. Acceleration vs. time for
one-dimensional end drop test analysis.

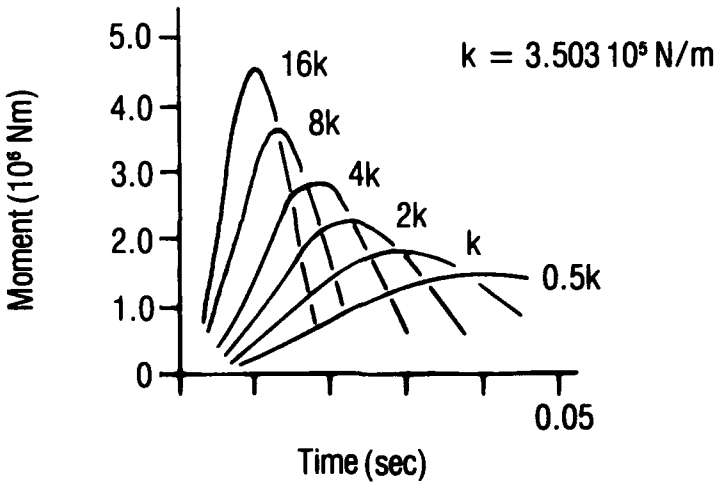

Figure 20. Ground moment applied to shelter for one-dimensional end drop test analysis.

L = Length of shelter (6.096 m)

x_0 = Location of center of gravity (3.048 m)

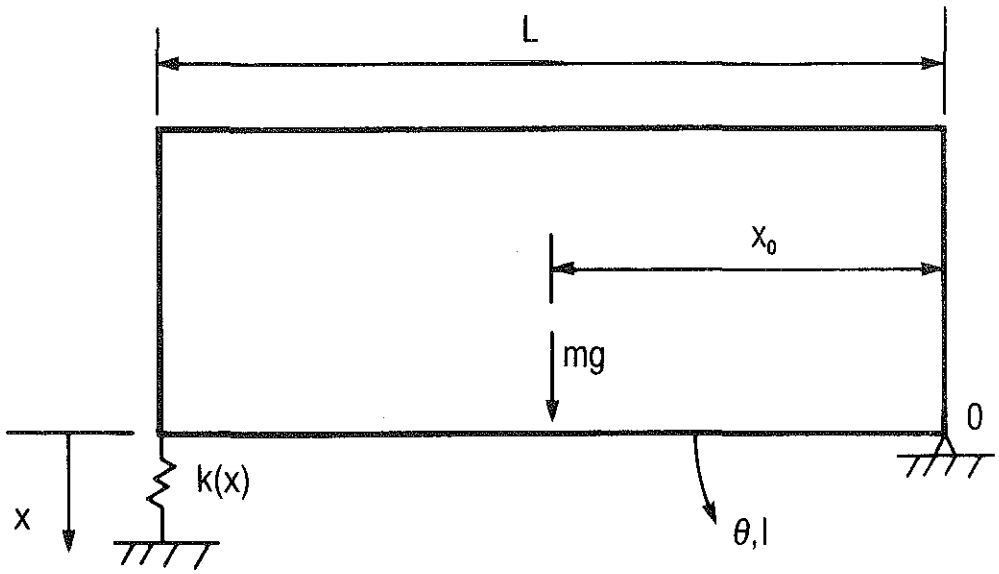

θ,x = Coordinates

m = The mass of the shelter ($6.645\ 10^3$ kg)

I = Moment of inertia about 0 ($8.589\ 10^4$ kg m^2)

k(x) = Variable spring constant

g = Acceleration due to gravity

Figure 21. Variables for one dimensional analysis of end drop test, ground modeled as a spring.

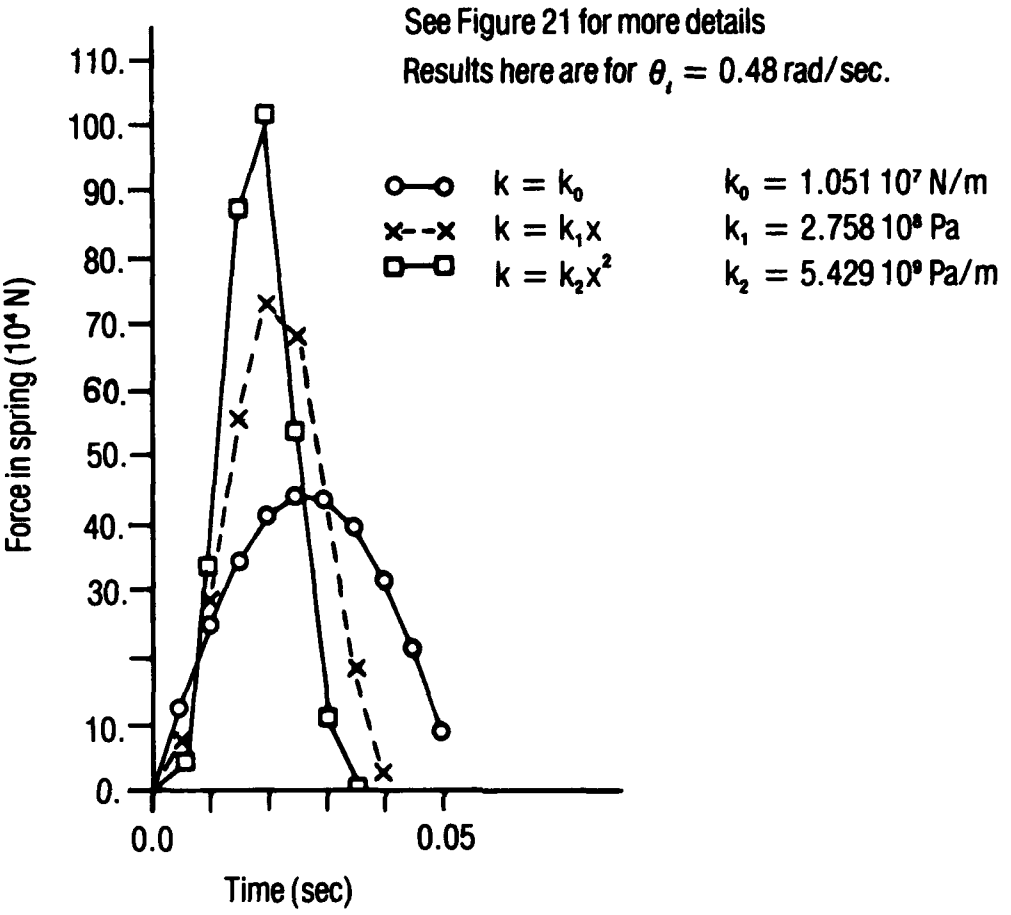

Figure 22. Force in spring vs time from analysis of end drop on spring of variable stiffness.

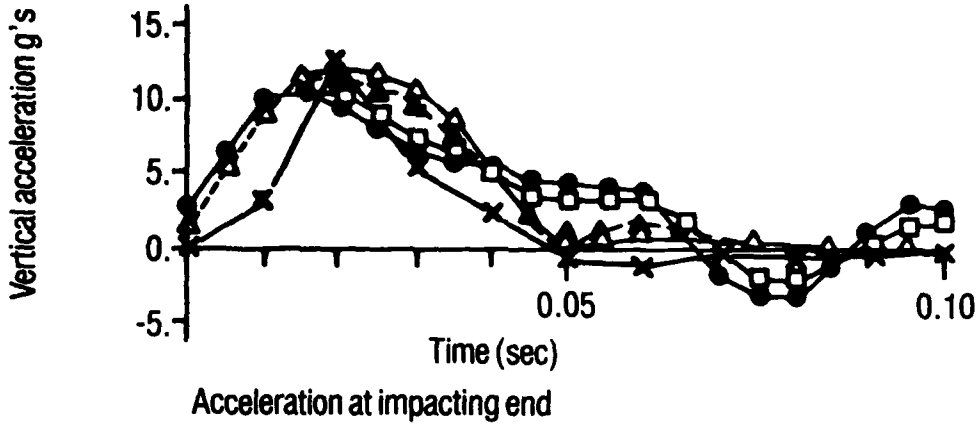

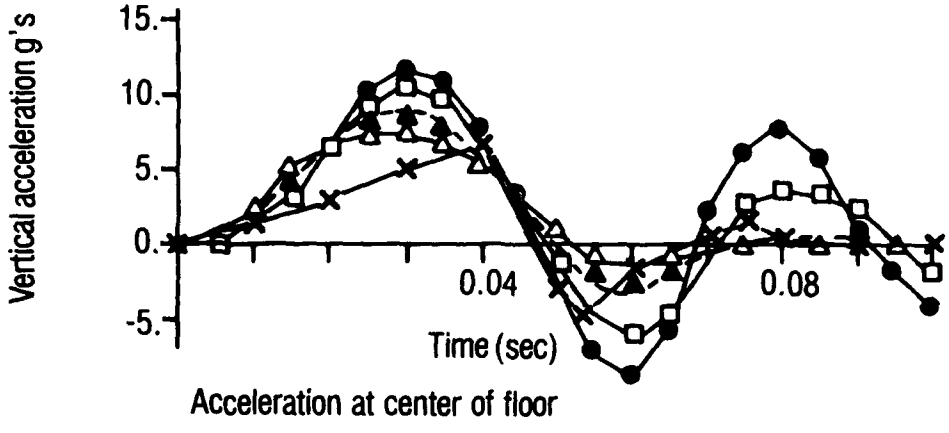

x Experimental
• Finite element, no damping, $\Delta t = 0.0050$ sec
◘ Finite element, damping $= 0.0010\,[k]$, $\Delta t = 0.0050$ sec
▲ Finite element, damping $= 0.0063\,[k]$, $\Delta t = 0.0050$ sec
--- Finite element, damping $= 0.0063\,[k]$, $\Delta t = 0.0025$ sec
Δ Finite element, damping $= 0.0100\,[k]$, $\Delta t = 0.0025$ sec

Figure 23. Acceleration vs. time at impacting end and center of floor, experimental and finite element for different damping matrices and time steps.

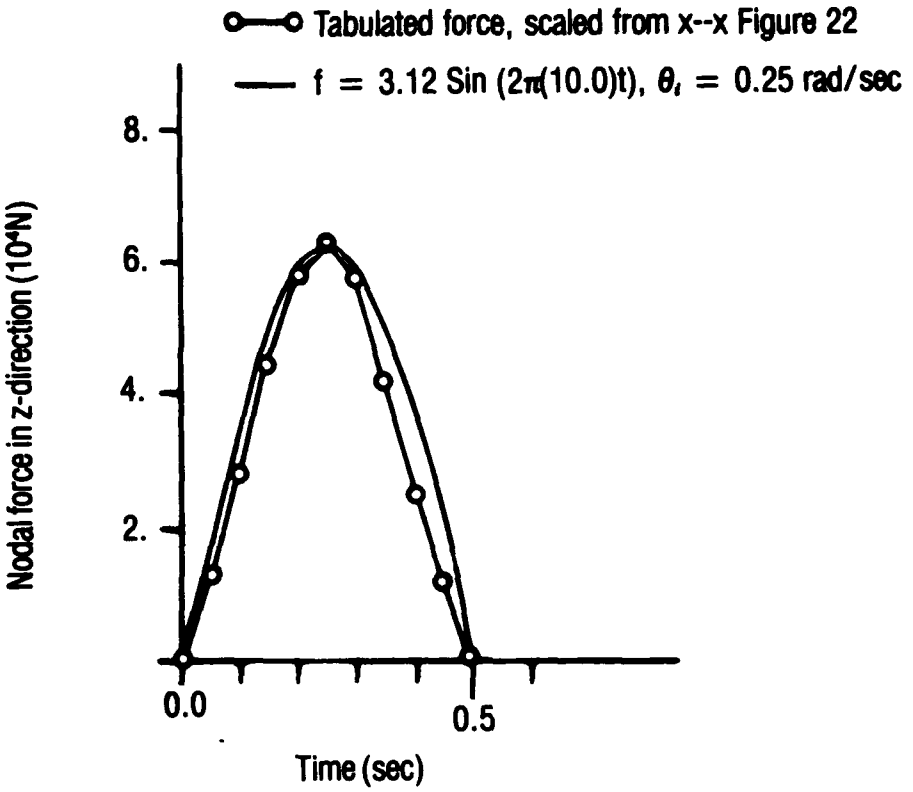

Figure 24. Force profiles of tabulated and harmonic loads; harmonic load was used as input to finite element analysis for end drop.

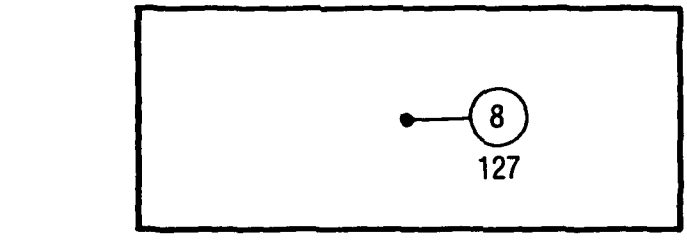

Fixed roof

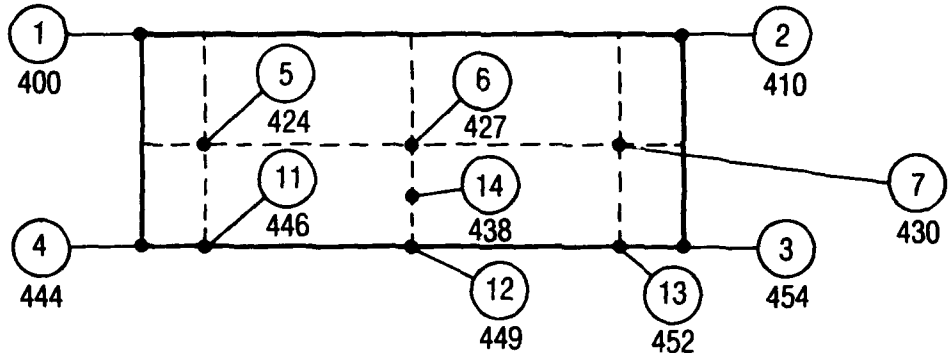

Fixed floor

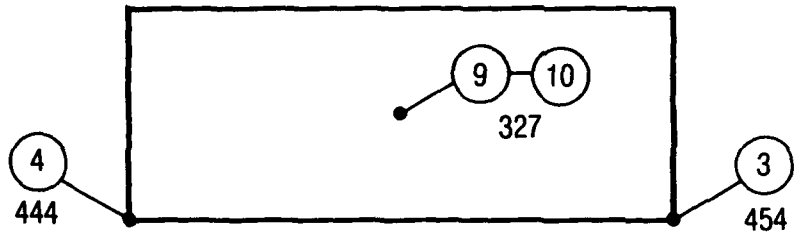

Expandable side

Figure 25. Location of points where accelerations were measured for the end drop test.

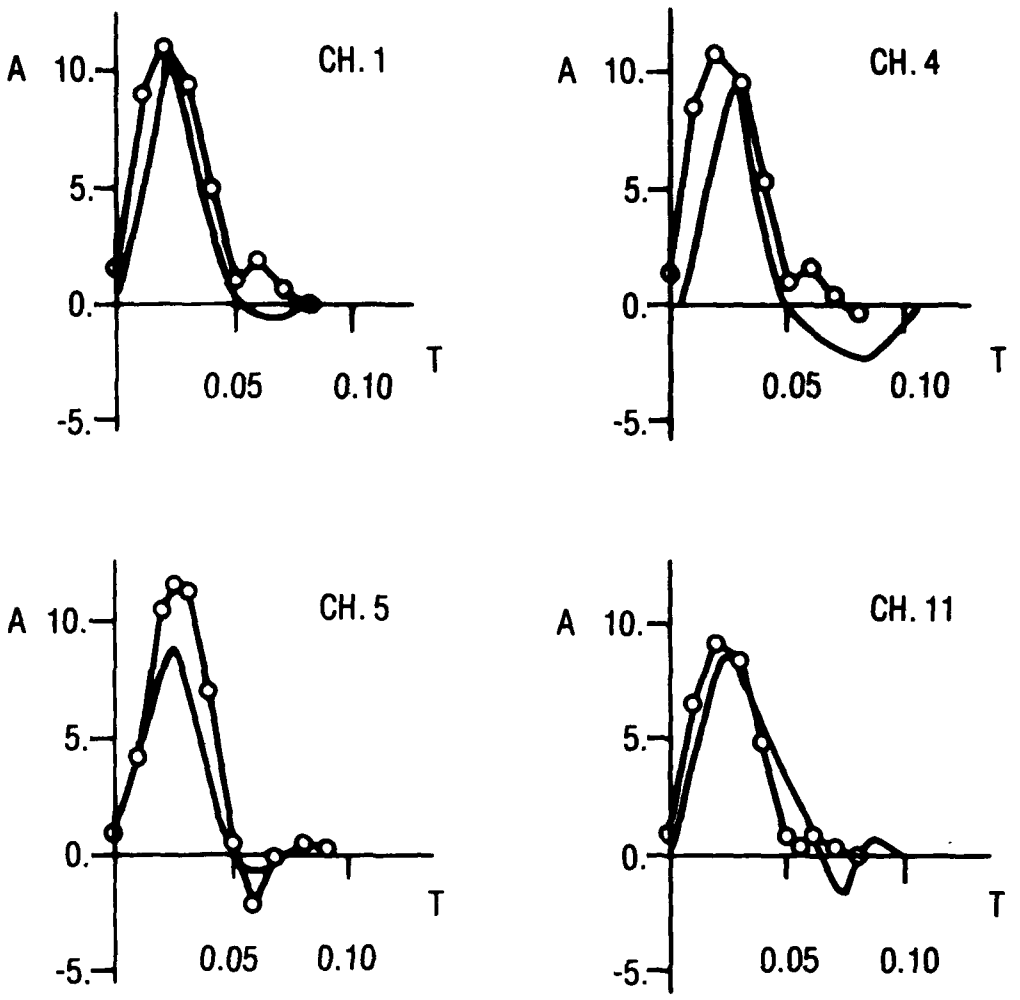

A = Acceleration (g's)
T = Time in seconds
—— = Measured data
—o— = Computed, F = A Sin (wt + ø),
ϱ = 0.0063, Δt = 0.0050

Figure 26. Acceleration vs time, end drop, channels 1, 4, 5, and 11.

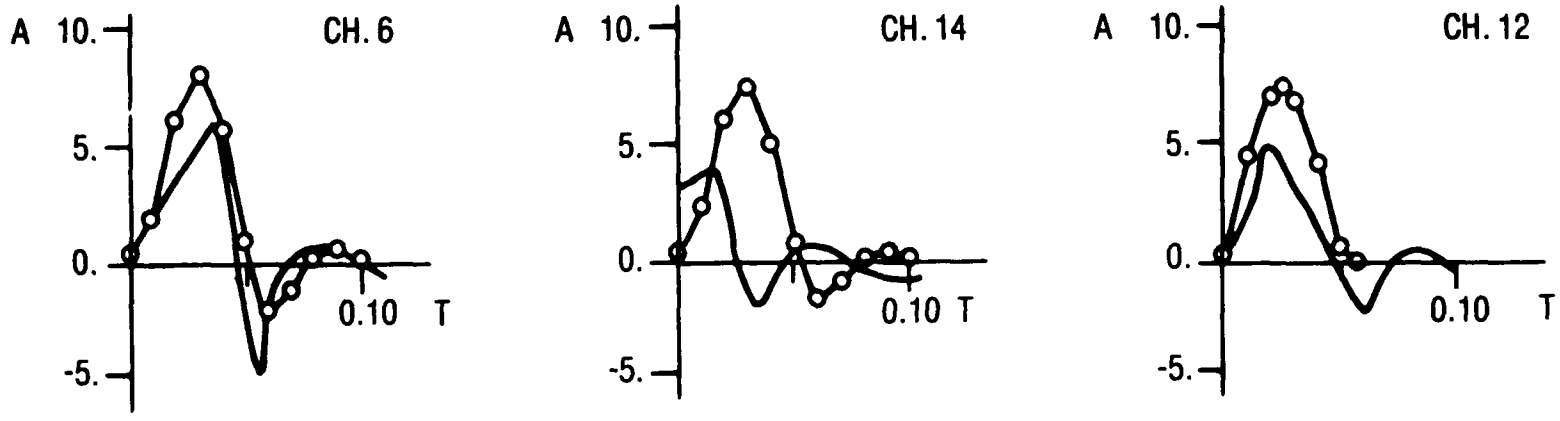

g

A = Acceleration (g's)
T = Time in seconds
— = Measured data
—o— = Computed, F = A Sin (wt + ∅), ϱ = 0.0063

Figure 26. Continued.

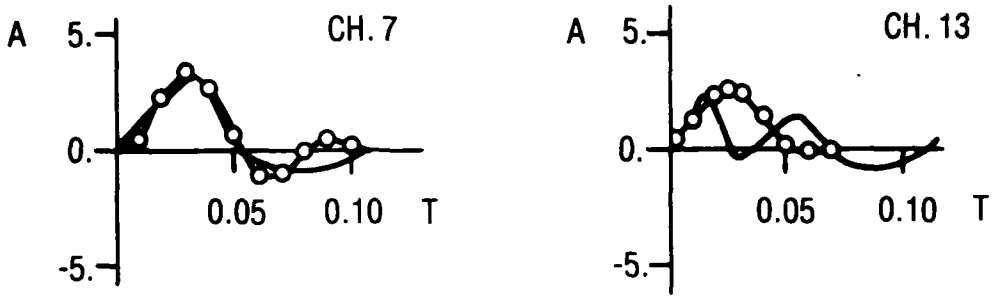

A = Acceleration (g's)
T = Time in seconds
— = Measured data
—o— = Computed, F = A Sin (wt + Ø), ϱ = 0.0063

Figure 26. Continued.

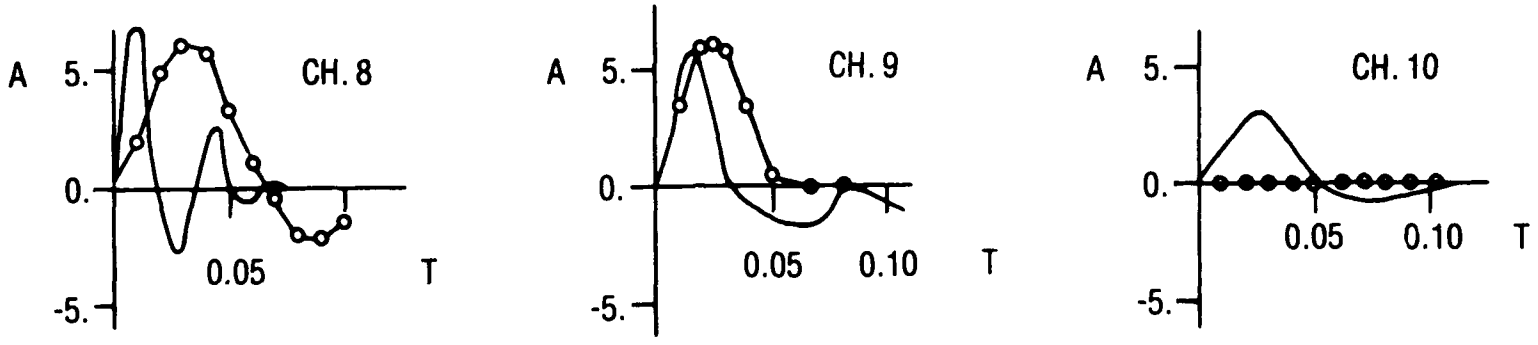

A = Acceleration (g's)

T = Time in seconds

— = Measured data

—•— = Computed, $F = A \sin(wt + \varnothing)$, $\varrho = 0.0063$

Figure 26. Continued.

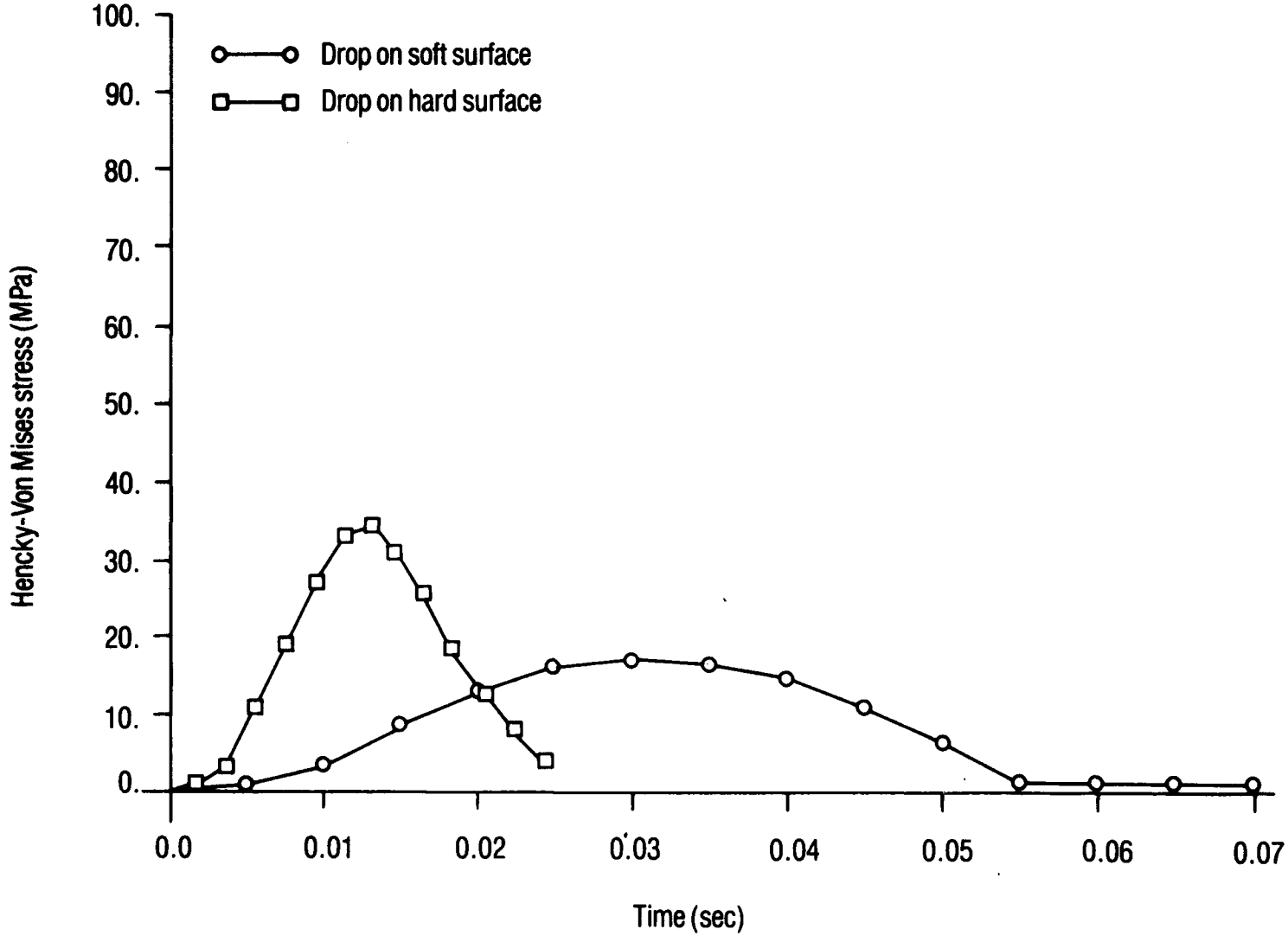

Figure 27. Henckey-Von Mises stress vs time in top skin at center of element no. 420 for end drop on both soft and hard surfaces.

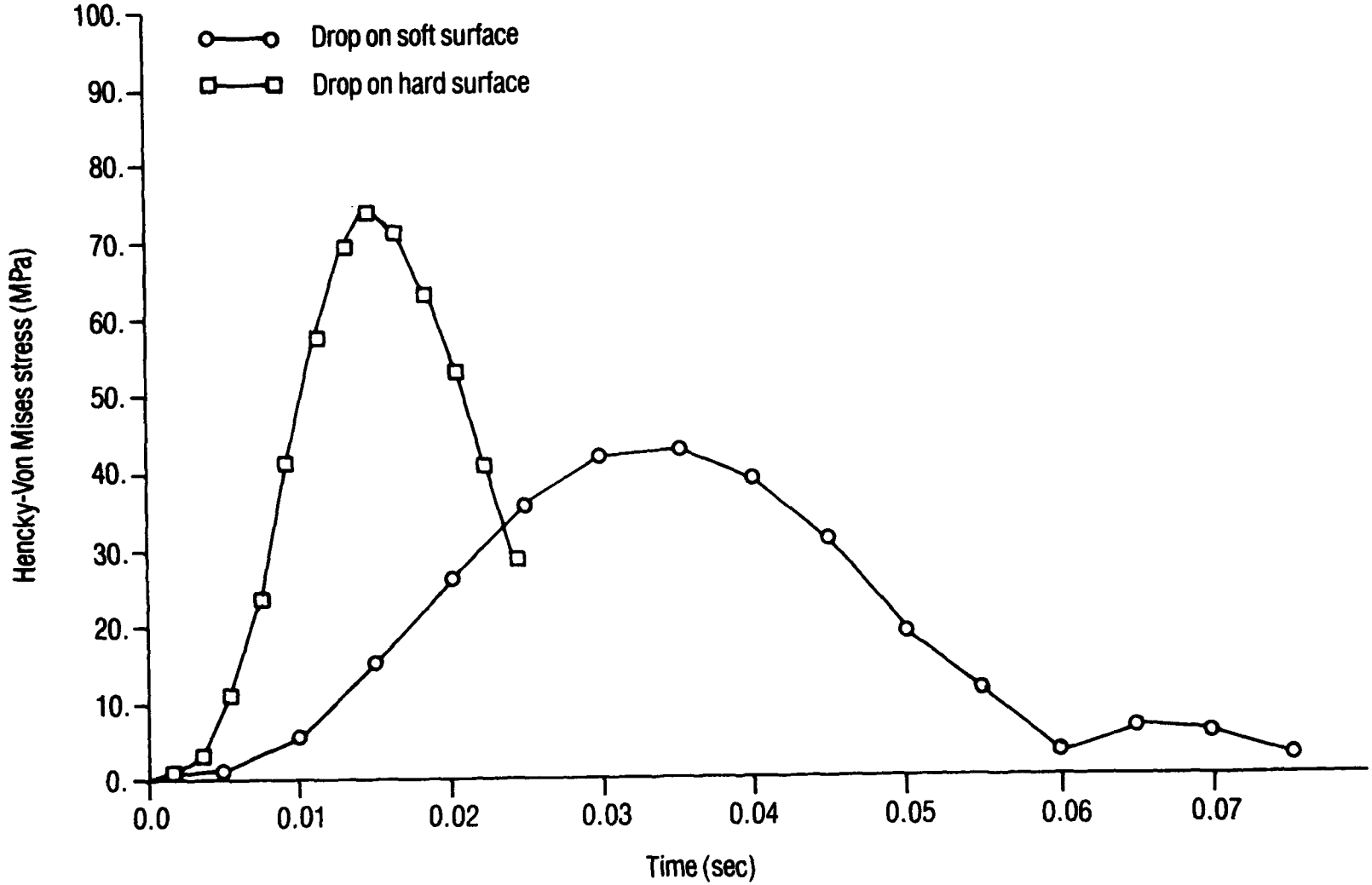

Figure 28. Henckey-Von Mises stress vs time in top skin at center of element no. 424 for end drop on both soft and hard surfaces.

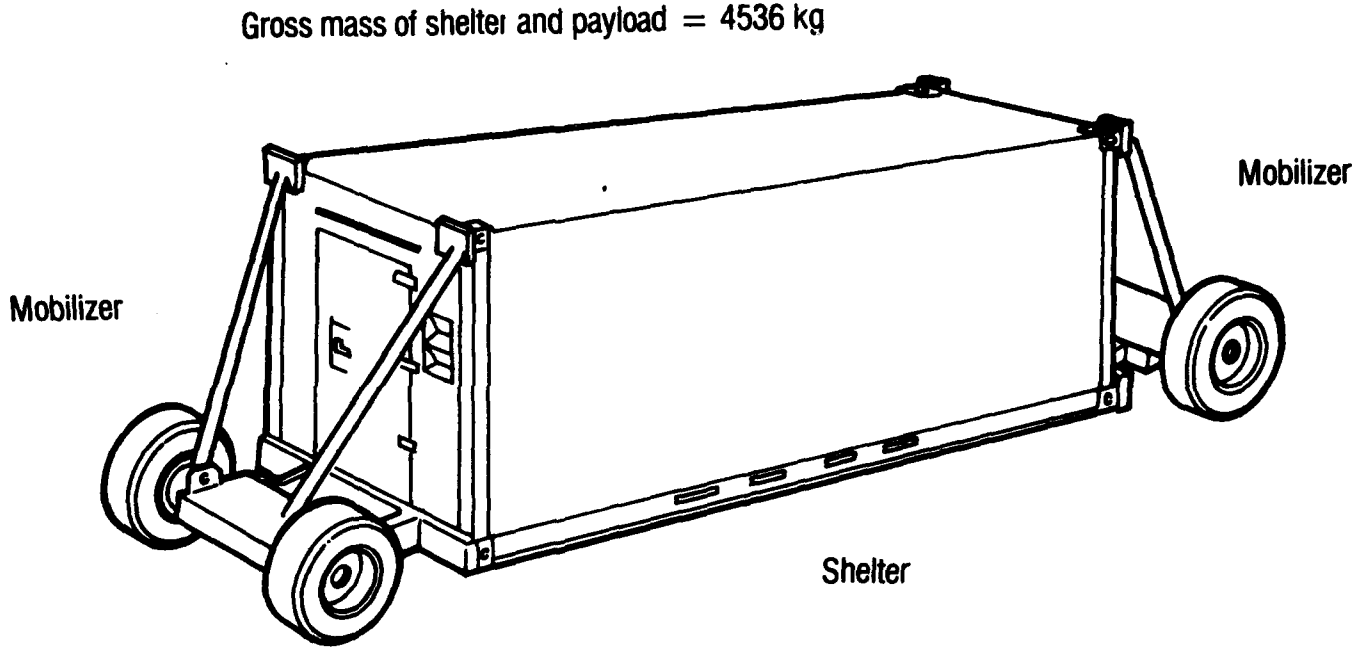

Figure 29. Shelter on mobilizers.

(N) = Channel number of accelerometer

NNN = Finite element node number

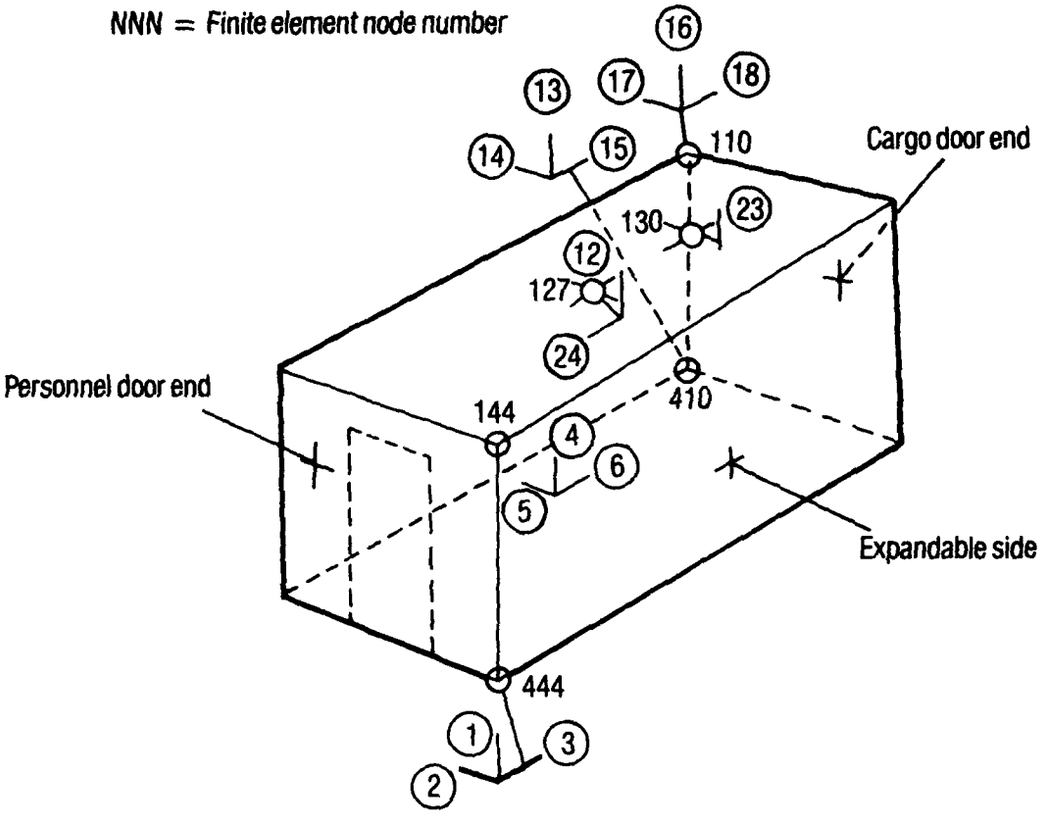

Channel Number	Location	Direction of Acceleration
1, 4, 13, 16	ISO fittings	vertical
2, 5, 14, 17	ISO fittings	transverse
3, 6, 15, 18	ISO fittings	longitudinal
12, 24	center of roof	vertical, longitudinal
23	center of roof on longitudinal center of roof	vertical

Figure 30. Location of experimental data points for Belgian block test.

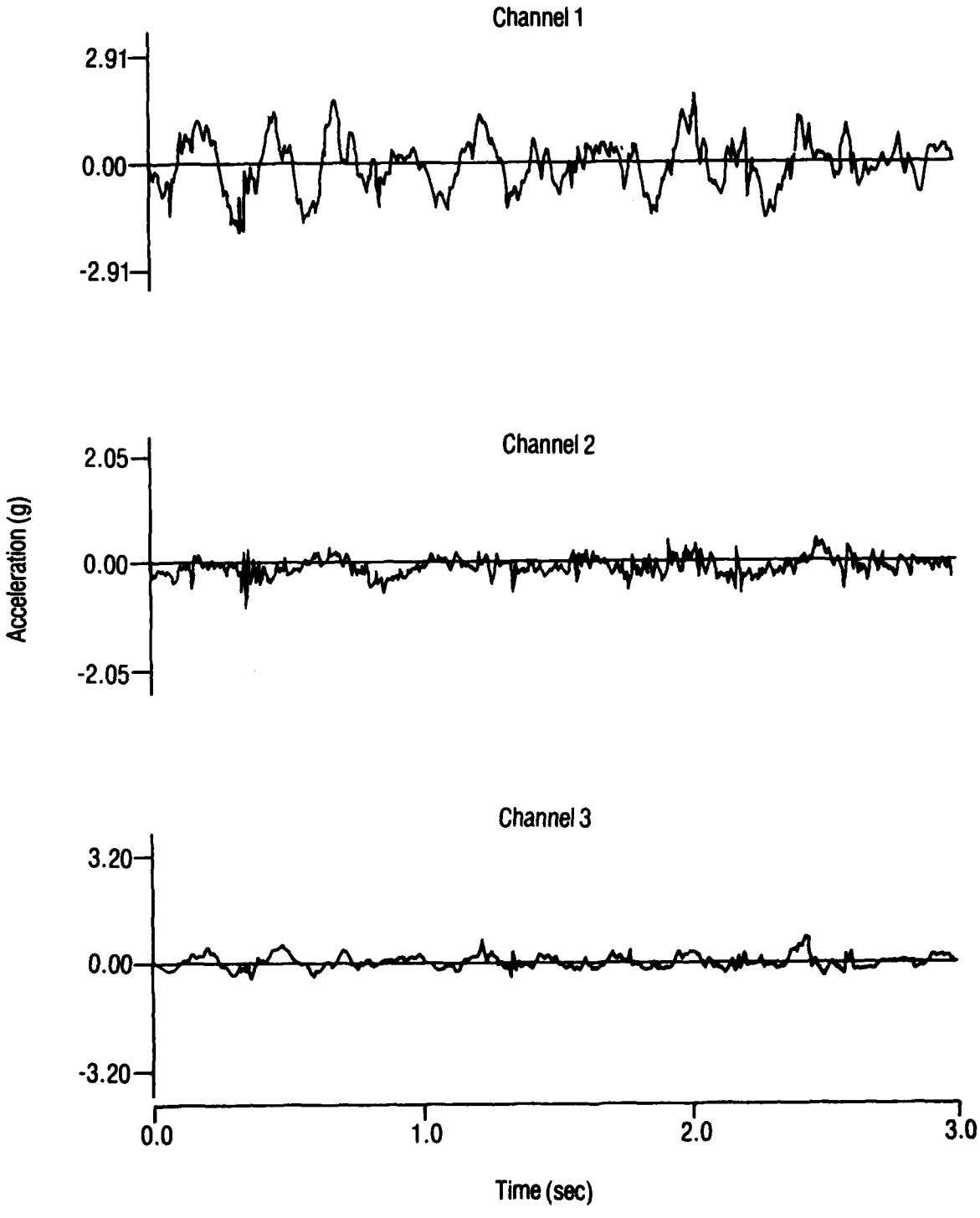

Figure 31. Acceleration vs time, Belgian block test, channels 1, 2, and 3.

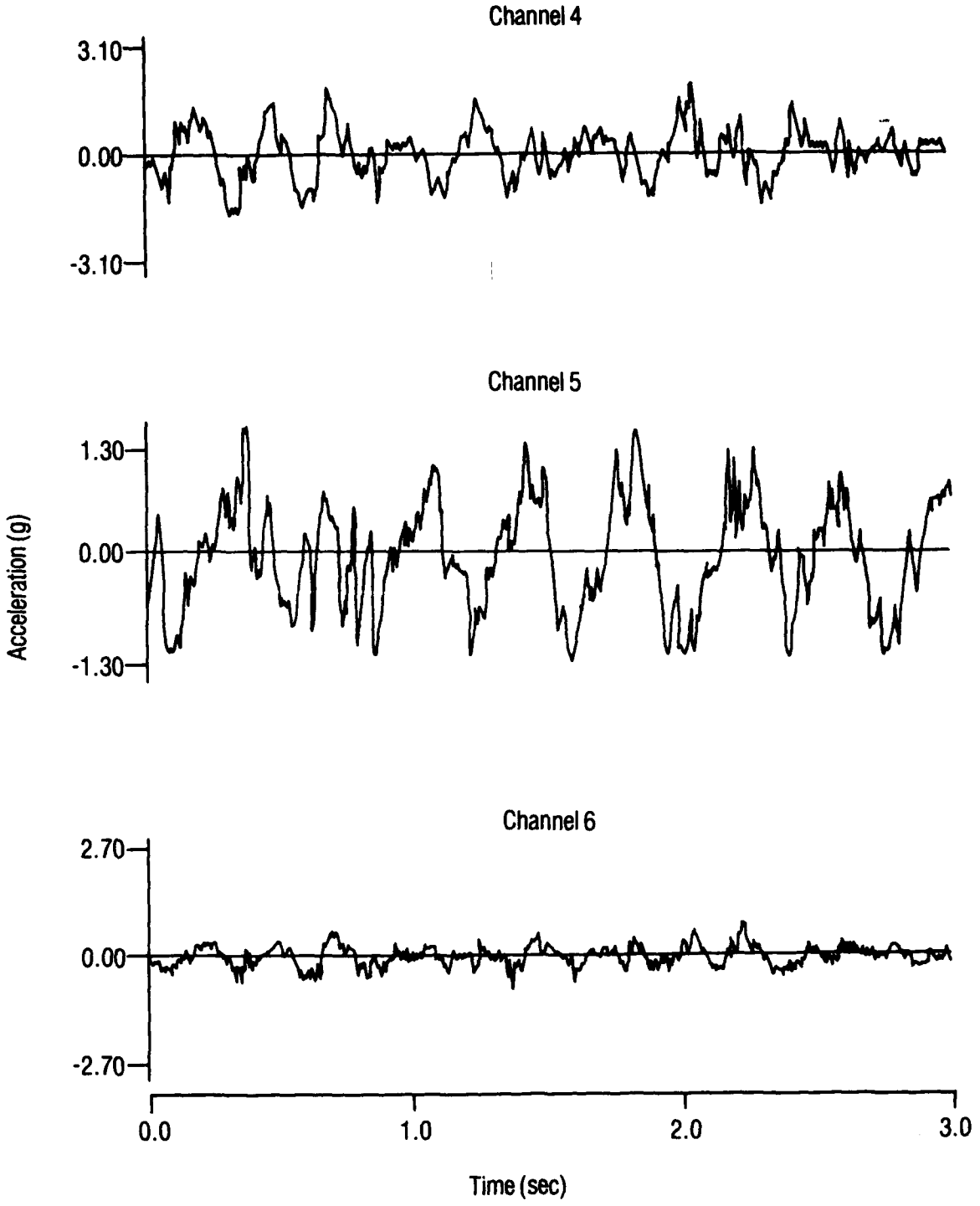

Figure 31. Contiued. Acceleration vs time, Belgian block test, channels 4, 5, and 6.

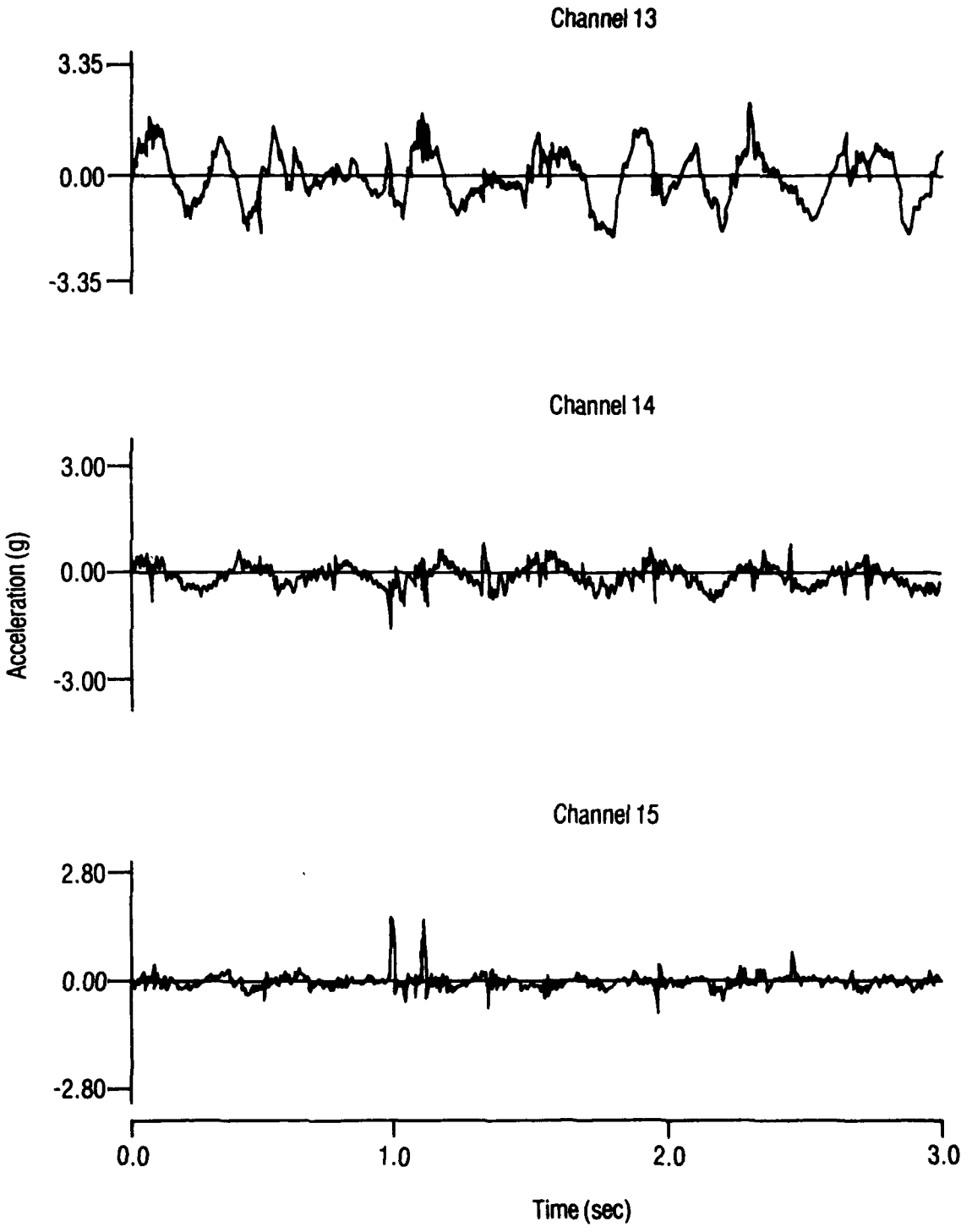

Figure 31. Continued. Acceleration vs time, Belgian block test, channels 13, 14, and 15.

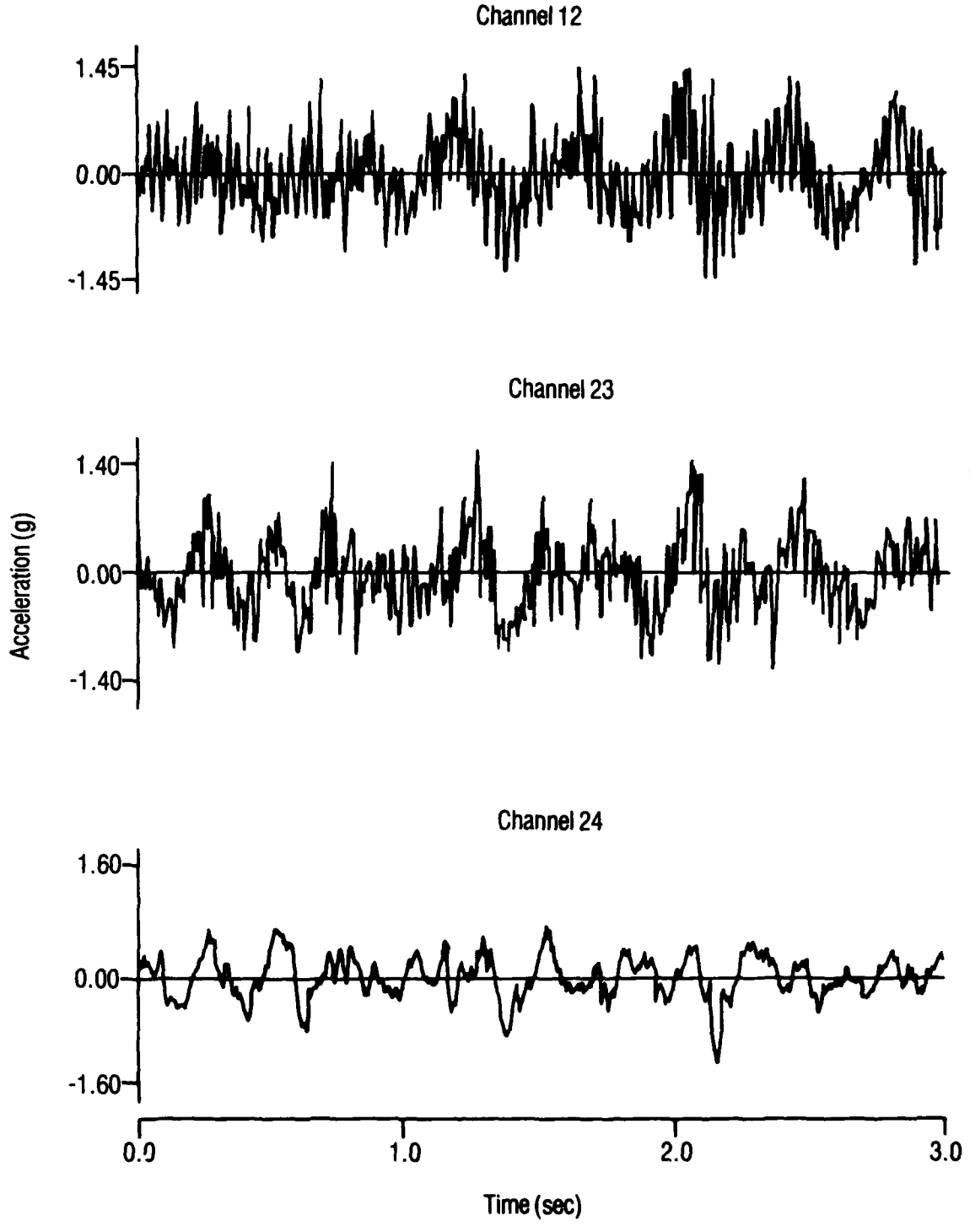

Figure 31. Continued. Acceleration vs time, Belgian block test, channels 12, 23, and 24.

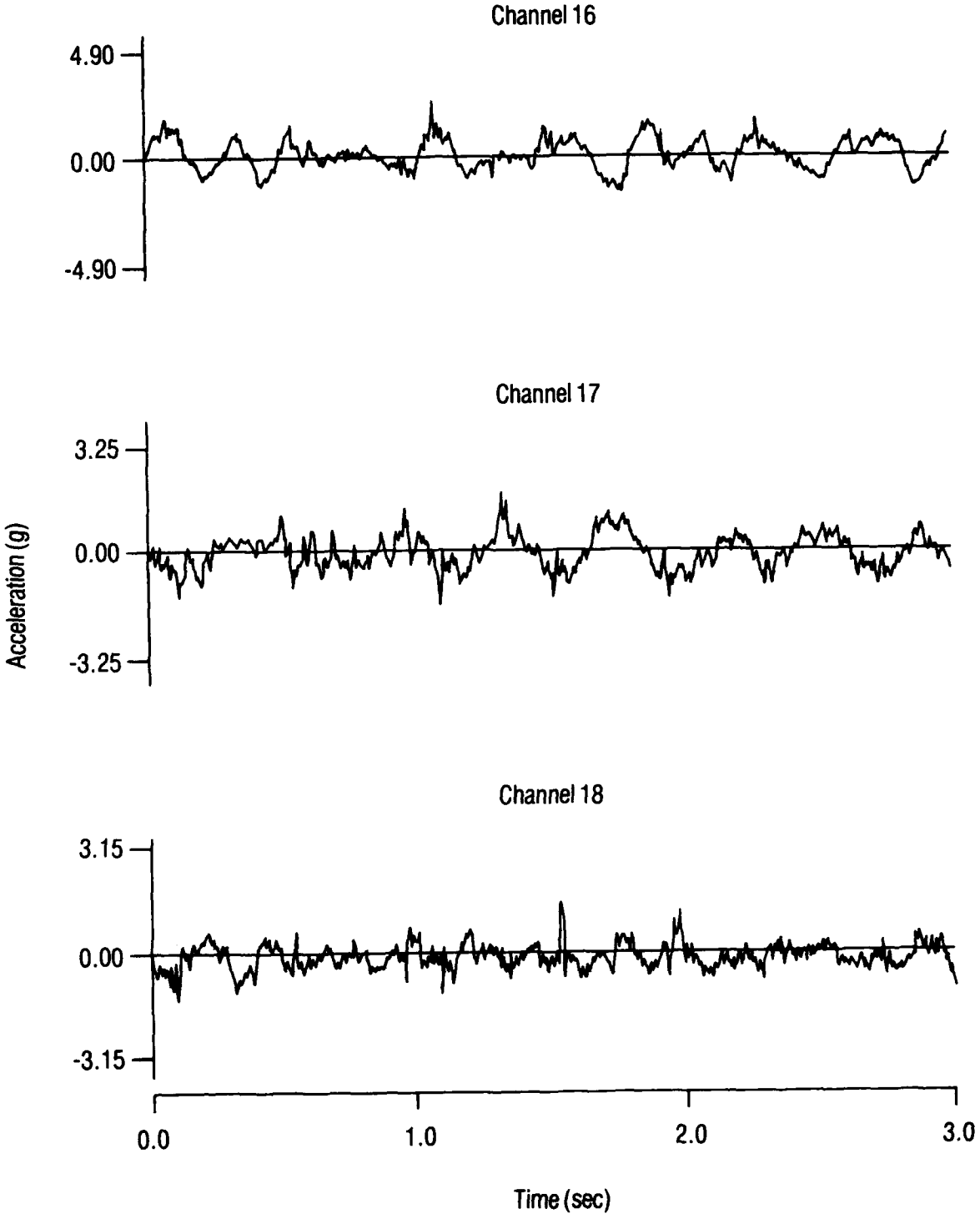

Figure 31. Continued. Acceleration vs time, Belgian block test, channels 16, 17, and 18.

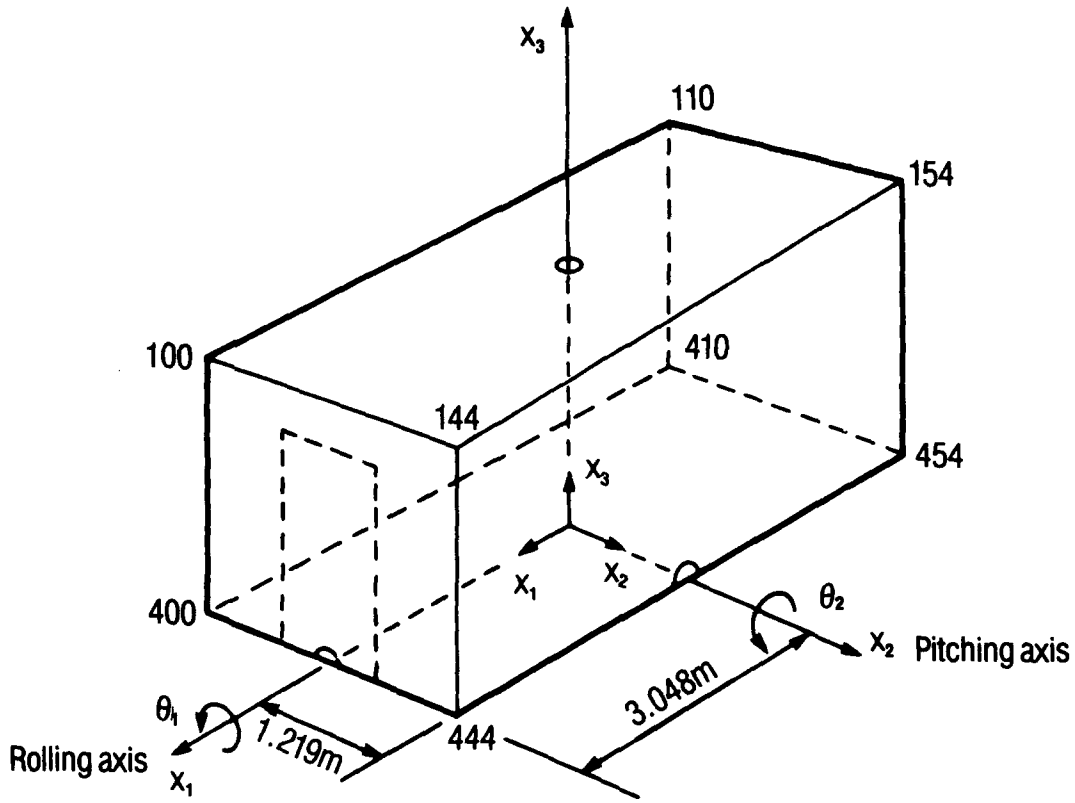

θ_1 = Rolling acceleration
θ_2 = Pitching acceleration
NNN = Finite element node number at which an ISO fitting is located.
X_1 = Unit vectors

Figure 32. Coordinate system for pitching and rolling accelerations.

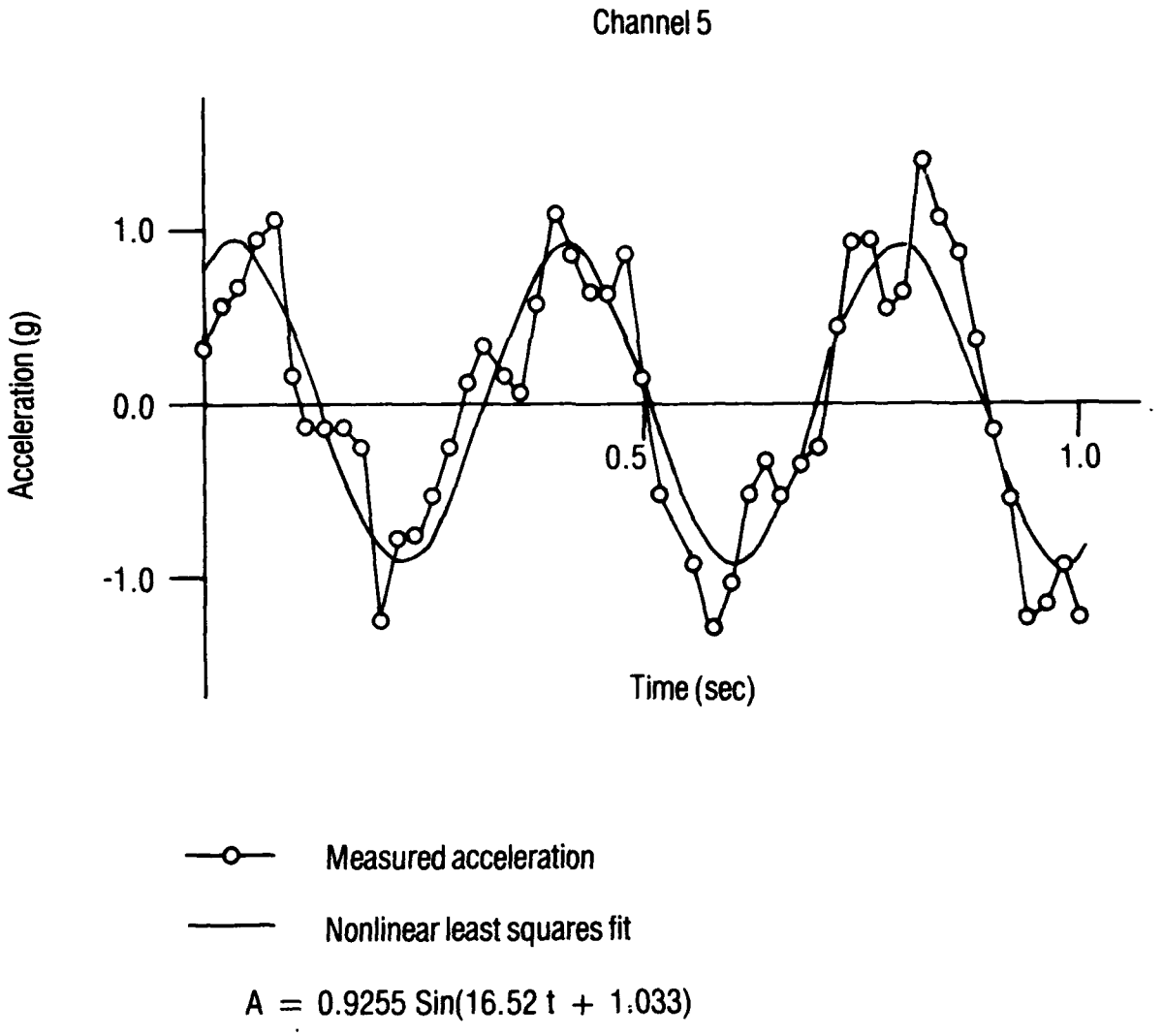

Figure 33. Nonlinear least squares fit for accelerations measured at channel 5.

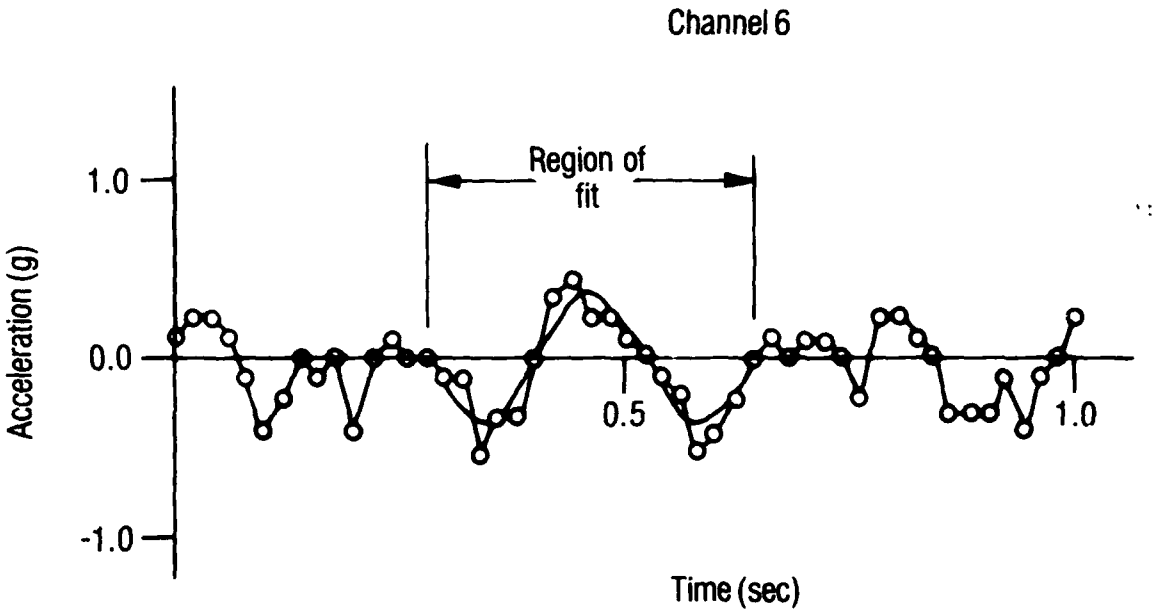

Measured Acceleration

Nonlinear least squares fit

$A = 0.3784 \, Sin(26.41 \, t + 1.933)$

Figure 34. Nonlinear least squares fit for accelerations measured at channel 6.

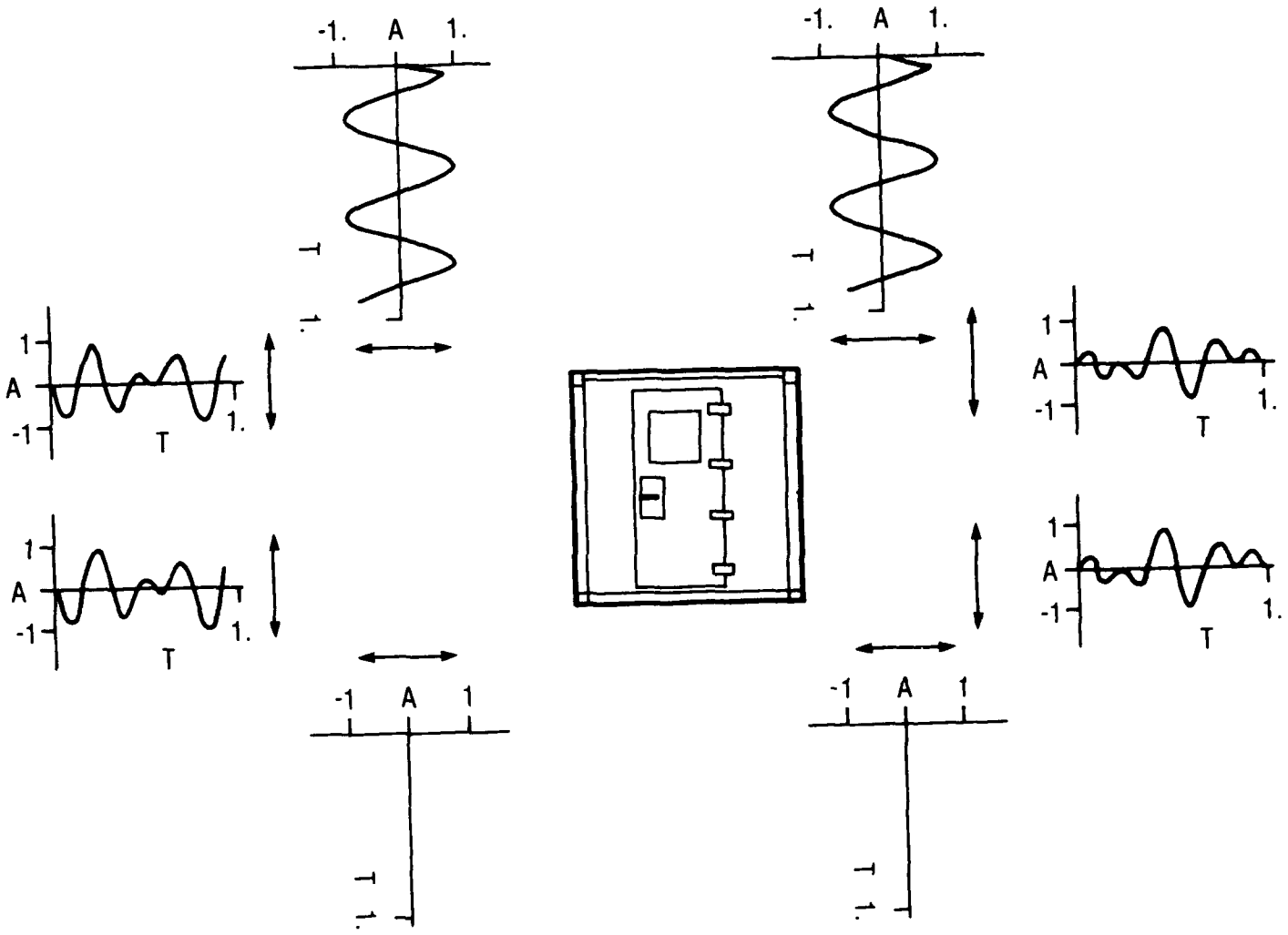

Acceleration (A) in g's, time (T) in seconds.

Figure 35. Rolling and pitching accelerations at ISO fittings, personnel door end.

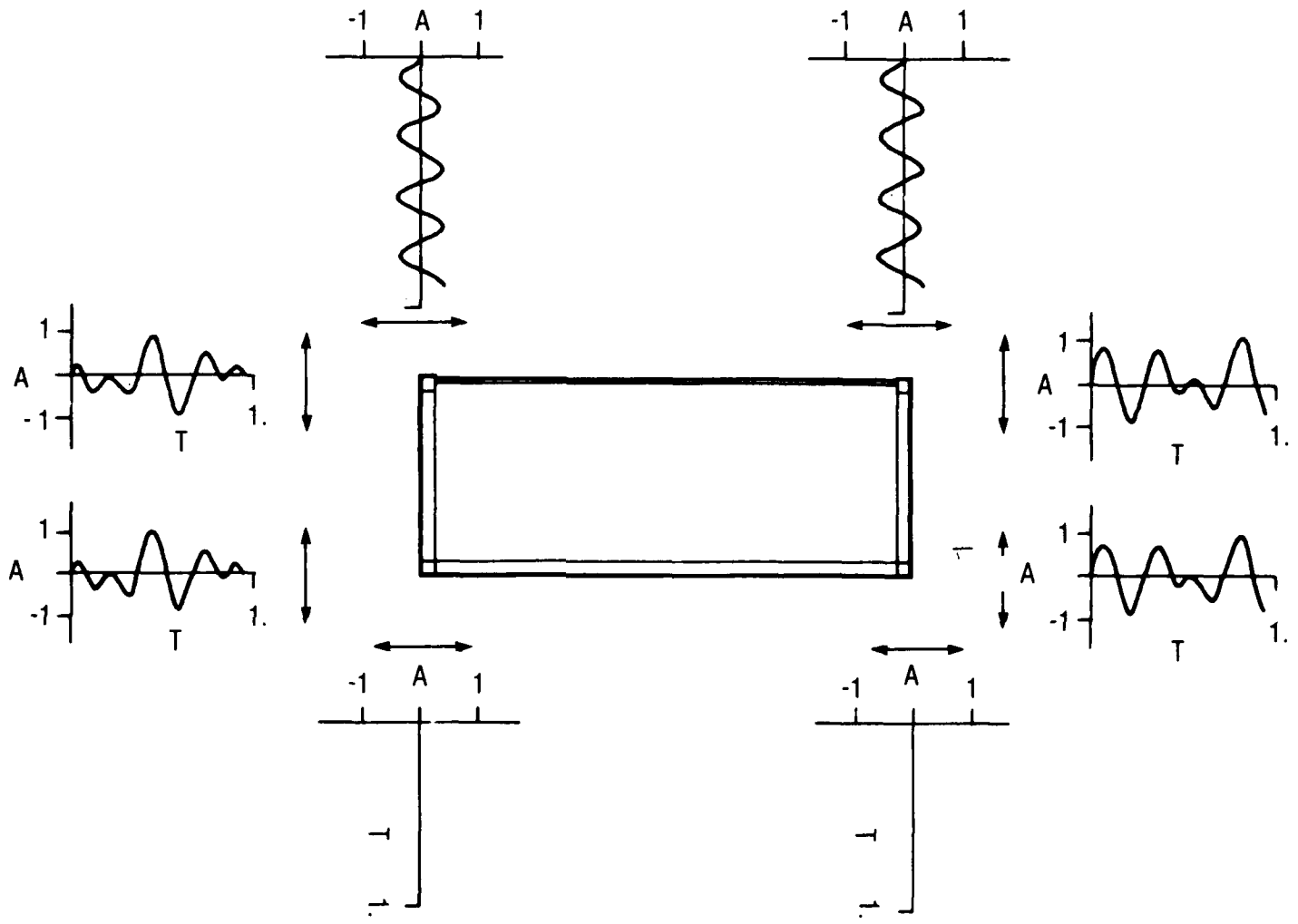

Acceleration (A) in g's, time (T) in seconds.

Figure 36. Rolling and pitching accelerations at ISO fittings, fold out floor side.

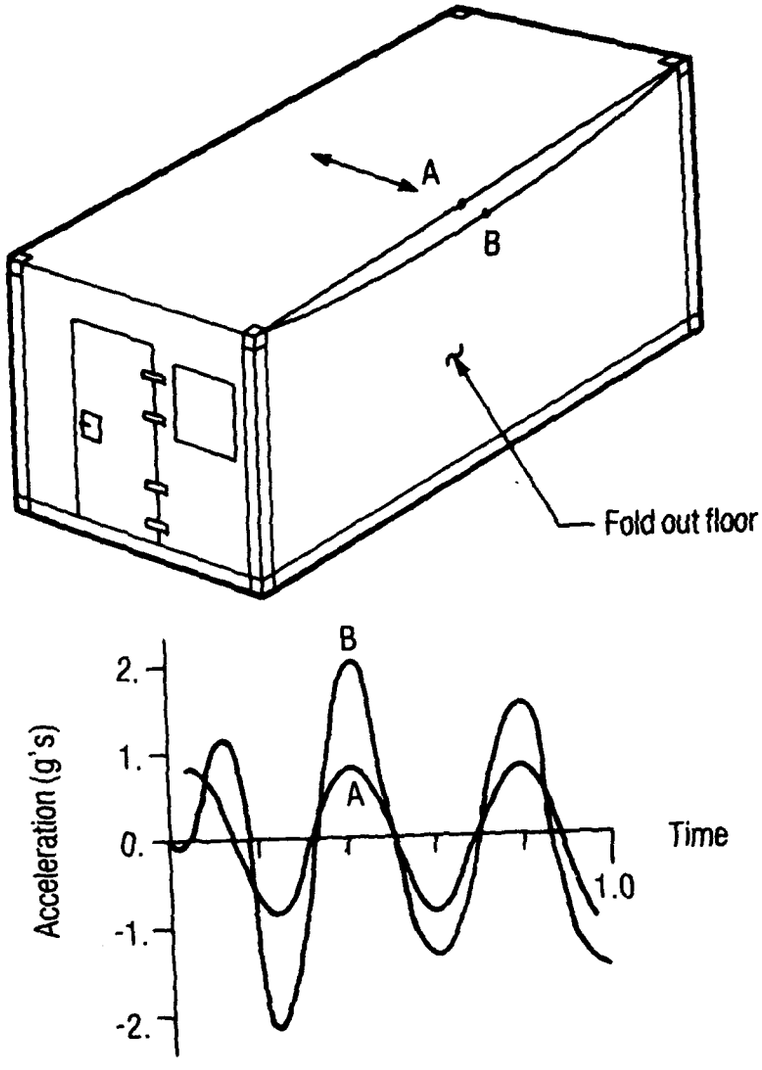

Figure 37. Elastic acceleration of fold out floor.

Table 1. Total mass of each structural panel

Panel	Mass (kg)
Fixed roof \	196.
Fixed wall	157.
Fold-out floor	178.
Fixed floor	225.
Personnel door endwall and door	94.
Cargo doors	39.

Total mass of structural panels = 889. kg

Table 2. Description of concentrated mass elements

Element No.	Node	Mass (kg)	Description
170	100	18.	ISO fitting top
171	110	18.	ISO fitting top
172	144	18.	ISO fitting top
173	154	18.	ISO fitting top
450	400	42.	ISO fitting bottom
451	410	42.	ISO fitting bottom
452	444	42.	ISO fitting bottom
453	454	42.	ISO fitting bottom
1200	302	34.	Folding side wall
1201	304	34.	Folding side wall
1202	306	34.	Folding side wall
1203	308	34.	Folding side wall
1204	146	40.	Expanding roof
1205	148	40.	Expanding roof
1206	150	40.	Expanding roof
1207	152	40.	Expanding roof
1208	159	36.	Folding end wall (personnel end)
1209	169	36.	Folding end wall (personnel end)
1210	170	27.	Folding end wall (cargo end)
1211	174	27.	Folding end wall (cargo end)

Total concentrated masses = 662. kg

Table 3. Free body vibration mode frequencies under 35.0 Hz determined using finite element model

Mode No.	Frequency (Hz)	Comment
1	0.00	Rigid body mode
2	0.00	Rigid body mode
3	0.00	Rigid body mode
4	0.00	Rigid body mode
5	0.00	Rigid body mode
6	0.00	Rigid body mode
7	4.49	Fold-out floor
8	10.9	Fold-out floor
9	11.5	Roof
10	20.0	Fold-out floor
11	25.5	Roof, floor
12	26.4	Roof, floor, side wall
13	27.5	Roof, floor, side wall
14	29.1	Fold-out floor
15	31.0	Roof, floor, side wall
16	33.7	Roof, fold-out, floor, side wall
17	34.4	Roof, fold-out floor

Table 4. Computed accelerations for different values of the mass used to enforce the pitching and rolling motion

(1) $P = \frac{Miso}{M_s}$	Enforced acceleration at node 100 $\ddot{z}$ at t = 0.14 sec g's	Dynamic response acceleration at node 327 $\ddot{y}$ at t = 0.32 sec g's
0.936 10^{11}	0.7024564	0.9868791
0.936 10^{7}	0.7024560	0.9868790
0.936 10^{5}	0.7024211	0.9868761
0.936 10^{1}	0.7061586	0.9730407
0.936	0.6410798	0.8474199

Notes: (1) Miso = the mass at each ISO fitting (kg) used to enforce the acceleration, M_s = 1870 kg = the mass of the shelter less the ISO fittings.

(2) The values presented in this table were obtained before a problem was detected in the COSMIC*NASTRAN program. The phase angles were not being included in the dynamic load. The results, however, still indicate the effects of the ratio of the mass used to enforce motion to the mass of the elastic model.